2008:018

MASTER'S THESIS

Study of Rock Stress Orientation from Borehole Breakouts and its Correlation to Drill Parameters and Geology

Results from Boreholes KFM01B AND KFM02A of Forsmark Site Investigation, Sweden

Agbanu C. James

Luleå University of Technology

Master Thesis, Continuation Courses
Exploration and Environmental Geosciences
Department of Civil and Environmental Engineering
Division of Rock Mechanics

2008:018 - ISSN: 1653-0187 - ISRN: LTU-PB-EX--08/018--SE

PREFACE

This thesis is submitted in partial fulfillment of the requirement for Degree of Master of Science in Applied Geosciences and Mining. The work was carried out at the Division of Mining and Geotechnical Engineering at Luleå University of Technology, Sweden.

I would like to thank Swedish Nuclear Fuel and Waste Management Co. (SKB), Sweden, for providing all the data needed for this project, especially to Rolf Christiansson and Lennart Ekman for their various roles during this project.

Fulfilling this study was made possible by financial support received from the Swedish Institute in a form of a Guest Scholarship grant throughout my entire study period at Luleå University of Technology. Therefore, I owe many thanks to the Swedish Institute.

Thanks to Associate professor Maria Ask and Assistant professor Håkan Schunnesson for being great and wonderful supervisors, who gave this project a direction right from the inceptions. I am very grateful for having such wonderful and concerned supervisors. Your enthusiasms for this project work are highly appreciated.

I am indebted to Dr. Akande J.M; a senior lecturer at the Federal University of Technology Akure, Nigeria, who introduced me to Luleå University of Technology, Sweden.

I would also like to express my profound gratitude to Professor Erling Nordlund, the head of Division of Mining and Geotechnical Engineering at Luleå University of Technology, Sweden, who played a role as my teacher and my contact person at the university.

Special thanks go to my family, particularly my Mum, Dad and my sister Mrs. Njideka Omokeh for always believing in me.

To all friends I have made over the years in Sweden, hopefully our paths will cross again.

To Ms. Miriam Drakenberg, thanks for being a caring and a wonderful friend. I will eternally miss your company.

Last, but by no means the least, I would like to thank Mr. David Saiang and the family, Mr. Roy Nicholson and Mr. Thomas Villegas for all their numerous supports and encouragement.

Luleå, March 2008

Agbanu, C. James

ABSTRACT

Knowledge of in-situ stress orientation is crucial for the understanding of many processes in the Earth crust such as tectonic development, earthquake occurrence, and fluid transport along faults. In the Forsmark site investigation, the knowledge plays an important role in storage design and borehole stability. The borehole breakout method is an important indicator of stress orientations, particularly in aseismic regions and intermediate depths (< 5 km). Borehole breakouts are stress-induced ovalisations of the cross-sectional shape of the borehole wall. The ovalisation is caused by compressive shear failure on intersecting conjugate shear planes, resulting in piece of rock spalling off the borehole wall. This usually occurs when the borehole stress concentration exceeds that required to cause failure of the intact rock.

This thesis presents data from boreholes KFM01B and KFM02A that are part of Forsmark investigation site of the Swedish Nuclear Fuel and Waste Management Co (SKB). Two types of borehole geometry and image tools, borehole televiewer (BHTV) and borehole image processing system (BIPS), have been used to reveal the stress orientation using borehole breakout methods. The objectives of this report have been to: (1) determine the downhole orientation of horizontal rock stresses; (2) identify the zones of rock continuum; (3) study the influence of geology on rock stress orientation; and (4) correlate borehole breakouts with measurement while drilling (MWD) parameters.

The result from this study shows that borehole breakouts are common in both boreholes. In borehole KFM01B, borehole breakouts have been identified starting from 47 meters borehole length (mbl), continuing to 499 mbl. Borehole breakouts occupy 203.3 m of total 500 mbl, which corresponds to almost 41% of the entire logged borehole. Almost 85% of the identified borehole breakouts were identified in the borehole sections 113-270 mbl and 398-499 mbl, respectively. The majority of the identified borehole breakouts are shallow and have a limited failure depth. In addition, almost 50% of the identified borehole breakouts have their σ_H-orientation ranging between 138°-142°N whereas 38% have theirs within the interval 154°-166°N. The length weighted average σ_H-orientation is 146°±10°N, which corresponds to quality B according to the WSM ranking scheme, which is essentially assigned for a high quality borehole breakouts [*Zoback*, 1992].

In borehole KFM02A, borehole breakouts are detected over almost 29% of the borehole length between 99 to 1002 mbl. They were identified more in abundance, and with uniform orientation of maximum horizontal stress, σ_H within the interval 500-1002 mbl. The upper 500 mbl of borehole KFM02A is characterized by higher variability in the downhole distribution and orientation of borehole breakouts. The result also reveals that the σ_H-orientation determined from borehole breakout is ranging between 126°-66°N (that is to say that the minimum horizontal stress orientations,σ_h, is ranging within the interval 36°-156°N), with a dominating (89%) σ_H-orientation ranging between 135°-159°N. They suggest a length weighted average σ_H-orientation of 146°±18°N. This also results in quality B according to the WSM ranking scheme, which is essentially assigned to high quality borehole breakouts. Hence, both boreholes yield the same average

orientation with slightly higher variation in stress orientation in borehole KFM02A than in borehole KFM01B. This orientation is consistent with the σ_H-orientation previously obtained at the Forsmark site particularly with hydraulic fracturing techniques, regional stress data and relative plate motions. For example, the hydraulic fracturing method suggested that the orientation of the maximum horizontal stress at the site varies from 100° to 145°N, whereas regional stress data and relative plate motion suggested 140° and 142°N, respectively.

Continuous rock stress orientations as well as decoupling zones were identified in both boreholes, which were strongly correlated to the existing geology and structures at the site. In borehole KFM01B, a heterogeneous interval existed between 47-200 mbl, which corresponds to almost 31% of the logged borehole whereas the homogeneous (a zone of rock stress continuity) section existed between 200-500 mbl. Likewise, in borehole KFM02A, the heterogeneous interval (zones of rock stress discontinuity) existed between 113-499 mbl and also corresponds to about 43% of the entire cored part of the borehole whereas a homogeneous interval existed between 499-1002 mbl. The span of rock stress discontinuity in borehole KFM01B and KFM02A is about 12º and 24º, respectively. This may suggest that the stress field varies down the hole (i.e., discontinuous zones).

A remarkably good correlation is observed between the sections in both boreholes with scatter in orientation of borehole breakouts and deformation zones. The general observation indicated that deformation zone DZ2 (increased frequency of open fracture with several crushed zones) may have contributed to the scatter observed in the subsurface section 113 to 200 mbl in borehole KFM01B. Similarly, three deformation zones were suspected to have contributed to that of borehole KFM02A. The deformation zone DZ3 (increased frequency of both sealed and open fractures) was suspected to have contributed to the scatter in rock stress orientation observed from 174 to 190 mbl; whereas deformation zone DZ5 (increased frequency of sealed fractures but to a lesser extent of open fractures) may have contributed to the scatter from 296 to 310 mbl; and lastly; deformation zone DZ6 (a wide zone with increased frequency of both sealed and open fractures) may have contributed to the scatter from 419 to 499 mbl. Another plausible explanation for the scatter in orientation of borehole breakouts is the coexistence of several rock units in the boreholes and also the contact points where those rock units coexisted (coalesce). In such sections of two or several interlayered rock types, the compressive strength of the rock varies. An example is the contact between granite and amphibolite. One should expect fractures to be initiated especially at the contact point of such coexistence, since granite rock is a hard rock whereas amphibolite is a weaker vein.

Measurement while drilling (MWD) parameters were collected in borehole KFM02A. I have analyzed two 6 m long sections with and without borehole breakouts, from 419- 425 mbl and 735-741 mbl, respectively. The short lengths of analyzed sections combined with the rather complicated nature of MWD data collection makes it difficult to draw firm conclusions. Nevertheless, the results suggest that MWD parameters are sensitive to any rock discontinuity. Hence, MWD parameters depict the mechanical properties of the host rock as a result of strength variations. The general trend observed in the correlated

section in the borehole suggest that the water flow rate is directly proportional to the water pressure and inversely related to both rotation speed and penetration rate, while the rotation speed is held constant. This is probably because the deformation zone DZ6 is penetrated in the upper interval. It is expected that in such a zone that the rock strength should be decreased. This is absolutely in order with MWD parameters, decreasing trend in water flow and water pressure, with increasing trend in both rotation pressure and penetration rate is an indication of deep fractures at those points, which serves as conduits by which water or drilling fluid injected into the borehole to cool down the drill-bit and at the same time flush the drill cuttings to the surface are lost. This interval could as well impact less resistance to the drill.

TABLE OF CONTENTS

1.0 INTRODUCTION

The in-situ state of stress is a key rock mechanics factor related to the safety and stability of underground excavations [*Hakala et. al. 2003*]. When designing an underground excavation at a great depth, especially at high stress conditions, it is important to have a reliable knowledge of the in-situ state of stress, the rock strength, and critical stress states of intact rock, pre and post failure deformation behavior of rock and the rock mass quality [*Hakala et. al. 2003*]. This is to enable underground excavation to remain stable throughout its operating stage.

In line with the above mentioned objectives, the Swedish Nuclear Fuel and Waste Management Co. (SKB) is carrying out thorough site investigations at two localities in southern Sweden, Forsmark and Oskarhamn, for an underground deep repository for nuclear waste project.

Several factors like topography, presence of major fracture zones, rock type distribution, structure of the rock mass, occurrence of ore and groundwater capacity have been taken into consideration [*SKB* 2005].

In this thesis, geometrical data from two boreholes in Forsmark have been analyzed with the objective to find stress induced enlargements (e.g., borehole breakouts) [Bell and Gough, 1979] (Figure 1). Several rock stress measurement methods have been applied and analyzed in the area, including overcoring, hydraulic fracturing (HF), hydraulic tests on pre-existing fractures (HTPF), core disking analyses, and identification and characterization of borehole breakouts [*Lindfors et al.* 2004*; Sjöberg et al.* 2005*; SKB* 2005; Ask 2007; *Ask and Ask.* 2007].

A common limitation of all rock stress measurement methods except for the borehole breakout method is that they provide point-wise estimates of (part of) a local stress tensor that usually probes a small section of a borehole [*Ask and Ask*, 2007]. For overcoring, the test size is very small, and the results may be flawed by measurement-related errors [e.g. *Ask,* 2003]. In addition, overcoring measurements are sensitive to high stress concentrations that may lead to core disking of the overcore, which is a tensile failure [*Sano et al.* 2005]. Other limitations include that the measurement must be made near a free surface, and strain relief is determined over a very small area [*Zoback,* 1992]. *Engelder and Shar* [1984] argued that near surface measurements obtained by overcoring are often subject to affects of local topography, rock stress anisotropy, and natural fracturing. A drawback for the HF method is that the vertical stress is not measured (in near vertical boreholes; *Ito et al.* [1999] and *Rutqvist et al.* [2000] independently showed that the theory for calculation of maximum horizontal stress in hydraulic fracturing method is approximal). In a similar manner, *Ask* [2004] argued that the methods used to determine the orientation of fractures in the HF method (i.e., oriented impression packers, geophysical logging, or electrical imaging method) are questionable: for example, (i) that impression packers yield unsatisfactory results in strongly inclined boreholes and for test

sections with multiple fractures; (ii) that orientation of geophysical logs may not be able to allow detection of very small fractures; and (iii) that the electrical imaging may yield unsatisfactory results in certain rock types such as clay stones and salts. Other bottlenecks with the HF method may include depth and location of measurement. Several authors [e.g. *Zoback and Zoback,* 1980; *Scott,* 2001] point out that HF measurements at shallow depths in association with engineering works may show stresses influenced by the construction or shallow geological structures, and not reflects the tectonic stress field at the depth. HTPF on the other hand does not suffer from limitations associated with determination of maximum horizontal principal stress [*Cornet et al.* 2003]. However, determination of the stress components requires pre-existing fractures in different orientations, accurate determination of fracture orientation and subsequent inversion analysis of the data [*Sjöberg et al.* 2005].These authors argued that HTPF is not an ideal method for a site with a limited number of fracture orientations, or for a site with very low permeable fractures because that may inhibit fracture opening. For core discing, the formation of discs depends significantly on the properties of the rock and the magnitude of the stress in the borehole axial direction [*Stacey and Wasseloo*, 2002]. In addition, the authors argued that the type and technique of drilling *(*including the thrust), can significantly affect the occurrence of discing, and therefore could not be a reliable technique to quantify the magnitude of in situ stresses.

However, with the introduction of borehole televiewer into the SKB database, the orientation of horizontal stresses can be accurately interpreted using the borehole breakout stress measurement method [*Zoback et al.* 1985].

Kirsch [1898] was the first to show that an anisotropic stress field results in variation in the circumferential (tangential) stress around a circular opening (e.g. a borehole), with maximum and minimum stress concentrations in the directions parallel to minimum and maximum horizontal stress concentrations, respectively. This theory has helped explaining the occurrence of borehole breakouts in near-vertical boreholes. Borehole breakouts are zones of spalling and fracturing in opposite sides of a (near-) vertical borehole, which elongates its cross-section in the direction of minimum horizontal principal stress [*Bell and Gough,* 1979]. This method provides good information on the orientation of stresses, but is less well established for estimating stress magnitudes [*Al-Ajmi,* 2006]. An additional weakness with this method is that it requires a higher stress concentration than the compressional and tensional rock strength, respectively. As a result, borehole breakouts generally do not start until intermediate depths.

Zones of borehole breakouts can be detected on logging tools such as the four-arm caliper (also known as dipmeter), the borehole televiewer (BHTV), the formation microscanner (FMS), and formation microimager (FMI) [*Reynolds*, 2001; *Zoback et al.* 2003].

In comparison between the four-arm caliper tool to that of the imaging tools, *Reynolds*, [2001] argued that the four-arm caliper tool is mostly used in older oil wells, and has now been largely replaced by imaging tools. Furthermore, that the data obtained from imaging tools could more confidently identify borehole breakouts compared to that obtained from the four-arm caliper tool.

I have used two types of logging tools for detection of borehole breakouts, borehole televiewer (BHTV) and borehole image processing system (BIPS) tools. The analyses involved in borehole breakouts include determination of location, size, and orientation of borehole breakouts in the two boreholes. Correlation of borehole breakouts with measurement while drilling data (MWD) enables to determine if breakouts are associated with reduced compressive strength of the rock that could be detected in MWD parameter plots.

1.1 Objectives

This thesis consists of a detailed study on the occurrence of stress-induced features in boreholes KFM01B and KFM02A at the SKB Forsmark investigation site.

The primary objectives of this study are to:

1) **Determine the downhole orientation of the horizontal rock stress.** The orientation of horizontal stress is determined from BHTV data using the PC based program WellCAD Reader, version 4.0 build 729. Occasionally, BIPS data are used to verify/reject potential borehole breakouts and other features, and BIPS data are viewed with the PC-based program BIPS image viewer for window 95/NT, version 2.51;
2) **Identify the zones of rock stress continuum.** These zones are identified from plots of orientation of borehole breakouts versus depth. Intervals of the borehole with (semi-) constant orientation of borehole breakouts are considered as zones of rock stress continuum whereas intervals with scattered orientations of borehole breakouts are considered to show zones of rock stress discontinuum;
3) **Study the influence of geology on rock stress orientation.** This is obtained by correlating the variation in borehole breakouts orientation with the downhole lithology and structural geology (i.e. deformation zones) in each borehole; and lastly
4) **Correlate borehole breakouts with measurement while drilling parameters**. This is obtained by comparing the variation of five MWD parameters in two intervals of the borehole: The first interval covers a zone of borehole breakouts, whereas the second interval covers a zone without borehole breakouts. The five drilling parameters obtained during drilling are water flow, water pressure, rotation speed, rotation pressure, and penetration rate. The comparison gives insight of whether the MWD parameters influence the formation of borehole breakouts.

1.2 Limitations

The following limitations have been observed:

1) Boreholes KFM01B and KFM02A deviated 11° and 5°, respectively, from the horizon. Yet, the theory of vertical boreholes was applied [*Bell and Gough*, 1979]. There is a possibility of breakout orientation determined by BHTV to differ from true direction relative to magnetic north due to measurement errors introduced by the tool [*Mastin,* 1988].

2) The MWD parameters were only collected for borehole KFM02A, whereas that of borehole KFM01B was not available at the time of this report. There may be a possibility that the situation in borehole KFM02A may not be the same as in borehole KFM1B.
3) In making plots for correlation between borehole breakouts and MWD parameters, only two intervals were compared (the section of the borehole with a deep borehole breakout and the section without borehole breakouts). The major limitation with this selected interval is that this interval may not be a true representation of the entire section of the borehole. This is because the majority of borehole breakouts identified in the borehole are shallow borehole breakouts with a limited failure depth.
4) Lastly, the amount of data in the MWD parameters is so enormous that all the data could not possibly be plotted and analyzed at the same time. However, only the few selected sections in borehole KFM02A were studied in detail and consequently there were used to infer the entire borehole.

2.0 FORSMARK SITE INVESTIGATION AREA

2.1 Introduction

The Swedish Nuclear Fuel and Waste Management Co. (SKB) is solely responsible for developing a nuclear waste disposal program for Sweden's spent nuclear fuel. SKB is jointly owned by Swedish Nuclear Power Companies. It has overall responsibility for the back and end of the nuclear fuel cycle in Sweden, including transportation of fuel, the handling and disposal of radioactive waste and decommission of nuclear reactors.

SKB started site investigations in the year 2002 at two sites in Forsmark and Oskarhamn, respectively. The aim of the investigations is to find a site for a deep repository for nuclear waste. The detailed site investigation is being conducted by various specialists and includes studies of geology, rock mechanics, thermal properties, hydrogeology, hydrochemistry, transport properties, and surface ecosystems (including overburden, surface hydrochemistry and hydrology [*SKB* 2005].

The Forsmark site investigation is area is located in north Uppland about 170 km North of Stockholm, next to the Forsmark nuclear power plant. Site investigations that include drilling are concentrated to a 6x2 km large area next to the Forsmark nuclear power plant (See the black arrow in Figure 1 for the location of the SKB candidate area).

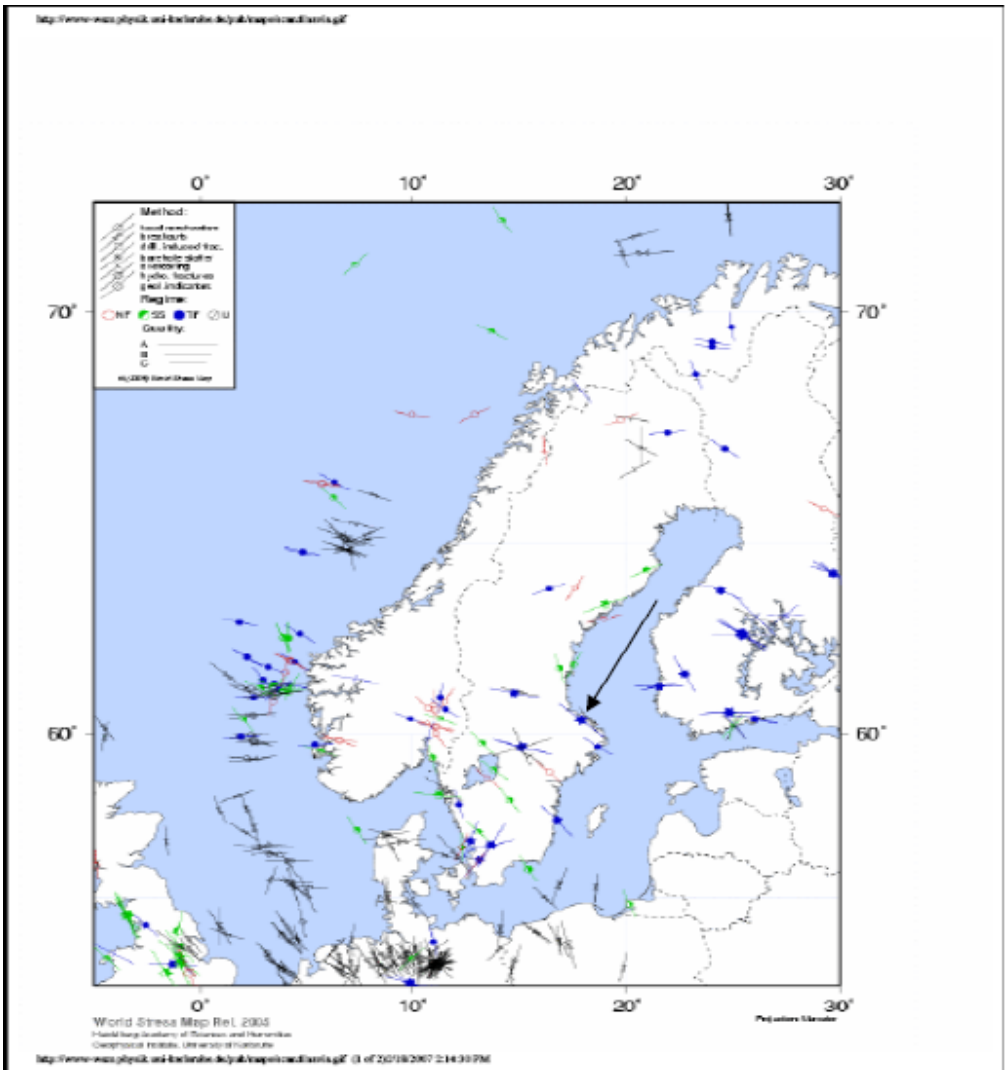

Figure 1: World Stress Map for Scandinavian showing different kinds of stress measurements [*Reinecker et al.* 2005]. The candidate area lies approximately at the black arrow point.

2.2 Geologic and tectonic settings

Forsmark is situated in the western part of the Paleoproterozoic Svecokarelian orogeny (Figure 2), inside the Fennoscandian Shield [*Juhlin and Stephens, 2006*]. The Forsmark area is part of a WNW-ESE to NE-SE striking deformation belt of the Svecokarelian orogeny that is several tens of kilometers wide [*Juhlin and Stephens,* 2006]. The bedrock is characterized by steeply dipping formations that are affected by high ductile strain. It is dominated by 1.89 to 1.86 Ga. old calc-alkaline plutonic rocks. The bedrock is folded around tectonic lenses, which generally are affected by lower ductile strain [*Juhlin and Stephens,* 2006]. The candidate area is located at the northwestern part of one of these tectonic lenses [*Juhlin and Stephens,* 2006]. The principal lithology in the candidate area is metagranite, which is cut by dikes, and minor intrusions of younger amphibolites (1.87-1.85 Ga) [*Juhlin and Stephens, 2006*]. Deformational structures in the metagranite include folds that are associated with development of strong, linear mineral fabrics

parallel to the fold axis lineation [*Juhlin and Stephens,* 2006]. The marginal areas of the tectonic lens generally show high ductile strain and a tectonic banding parallel to the strike of the rocks (Figure 2). This may signify that that the NW-SE striking zones may have greater regional importance than zones with WNW-ESE strike [*Juhlin and Stephens,* 2006]. The initial report by *Carlsten et al.* [2004a] suggested that borehole KFM01B could be referred to as single lithological rock unit. However, on the basis of fracture frequency, the author further subdivided the rock unit into two sections: (1) Medium grained metagranite-granodiorite with subordinate occurrence of fine-to-medium grained metagranitoid (RU1) and (2) Medium grained metagranite-granodiorite with subordinate pegmatitic granite, amphibolites and fine-to-medium grained metagranitoid (RU2). For detailed description of this unit, the reader is referred to Appendix 1.The author further suggested that three major deformation zones are intercepted by the borehole: (1) Section with several crushed zones and strongly increased frequency of open fractures with most common filling minerals as calcite, chlorite, and asphalt (DZ1); (2) section with increased frequency of sealed fractures with epidote and laumonite as dominant filling minerals (DZ2); and lastly, (3) section with two crushed zones and increased frequency of sealed fractures with calcite, laumonite, chlorite, and prehnite as dominant filling minerals (DZ3).

In borehole KFM02A, *Carlsten et al.* [2004b] subdivided the borehole into four lithological rock units (RU1-RU4). (Please kindly refer to Appendix 2 for detailed description of these rock units). But on the basis of fracture frequency, the borehole was further subdivided into sixteen rock sub-sections. Also, the author attributed ten deformation zones (DZ1-DZ10) to borehole KFM02A. (Please kindly refer to Appendix 2 for the detailed description of the ten deformation zones according to *Carlsten et al.* [2004b]).

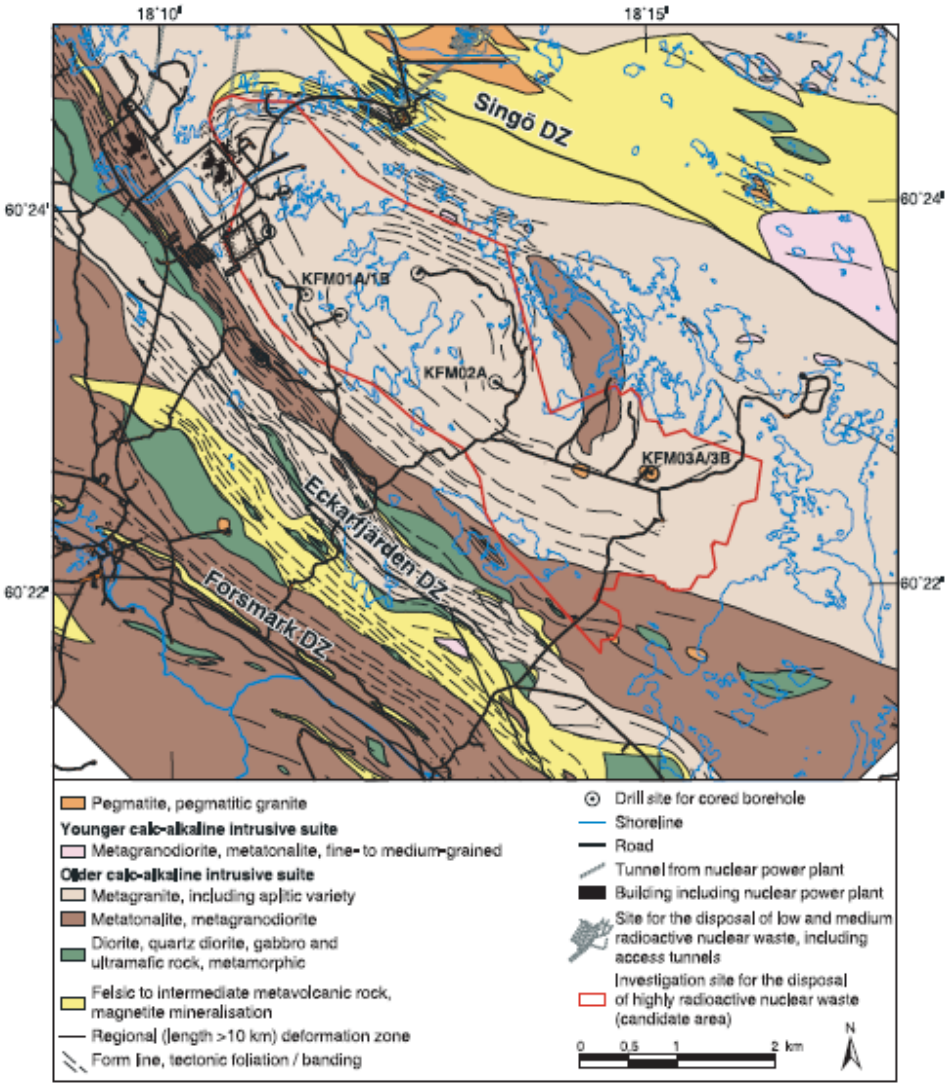

Figure 2: Showing the bedrock geological map of the Forsmark candidate area and the surrounding site and also the location of boreholes KFM01B and KFM02A [After *Juhlin and Stephens,* 2006].

2.3 Existing rock stress data

Figure 1 shows rock stress data from the World Stress Map (WSM). The WSM project of the International Lithosphere Programme was initiated in the year 1986 to compile and interpret data on the orientation of the in-situ stress field [*Zoback*, 1992]. The WSM project contains six types of different kinds of stress indicators e.g., borehole breakouts, drilling induced fractures, earthquake focal mechanisms, hydraulic fracturing, overcoring, and geological stress indicators (Figure 1).

The stress state at the Forsmark site has previously been assessed based on [*Sjöberg et al.* 2005]: (1) overcoring measurement, (2) stress estimation from core discing and spalling failure, (3) stress estimation from observed dicing of solid core, (4) selected data from hydraulic fracturing measurements, (5) overcoring stress measurements, including reinterpretation of the data using transient strain analysis and indirect stress estimates

from observed core discing, (6) hydraulic fracturing stress measurements, (7) other shallow measurements at Forsmark (near unit 3 and near SFR facility) and (8) regional stress data from Finnsjön, the Stockholm city area, Björkö, and Okiluoto, as well as data from Stress Map data and relative stress motion.

The result shows that the maximum horizontal stress within the Forsmark site is oriented NW-SE (140ºN) [e.g. *Sjöberg et al. 2*005]. This orientation is parallel with the overall direction of the tectonic lens and the associated regional deformation zones [*SKB 2005*]. Variations in stress orientation especially in the upper 100 to 200 m of the rock are assumed to be a result of local variability of the frequency and orientation of fractures and structures [*SKB 2005*]. The flat topography of the site is attributed to be the reason why the principal stresses are confined to the horizontal plane and vertical direction [*SKB 2005*].

2.4 Boreholes

2.4.1 Borehole KFM01B

Borehole KFM01B is included in drill site DS1, and was completed from 25th June 2003 to 15th January 2004 (Figure 1 and Figure 2). The borehole was originally drilled to compensate for missing core sections from 0-100 m in borehole KFM01A, as well as to perform rock stress measurements using the overcoring method [*Claesson and Nilsson*, 2005]. The borehole was drilled to a total length of 500.52 meter borehole length (mbl) and reaches 480 m in vertical distance from the ground surface [*Claesson and Nilsson*, 2005]. Borehole KFM01B has an azimuth and inclination of about 268º and 79º, respectively. For the detailed information on rock units and the deformation zones in borehole KFM01B, the reader is referred to Appendix 1, Sections 2.2 and Section 6.1.1)

2.4.2 Borehole KFM02A

Borehole KFM02A is included in drill site DS2, and was completed from November 2002 and March 2003 (Figure 1 and Figure 2). The main target for drilling the borehole was for chemical and microbiological investigations [*Claesson and Nilsson*, 2004]. The borehole was the second deep-cored borehole drilled in the Forsmark candidate area [*Ludvigson et al.* 2003]. Borehole KFM02A has an azimuth and inclination of about 276º and 85º, respectively. The borehole was drilled to a total length of 1002 mbl with telescopic drilling technique, where the upper 100 m is percussion drilled with the diameter of about 250 mm and the remaining interval, from say 100–1,000 m, is core drilled with the diameter 77.3 mm [*Rouhiainen and Pöllänen*, 2004]. The interval 0 -100 m is cased with the inner diameter 200 mm (For the detailed information on rock units and deformation zones in borehole KFM02A, the reader is referred to Appendix 2, Sections 2.2 and Section 6.1.2)

3.0 BOREHOLE BREAKOUTS

3.1 Brief borehole breakouts history

Haimson and Herrick [1985] reported that one of the earliest observations of what later would be known as borehole breakouts was made by *Leeman* in 1964 in the Witwatersrand deep gold mine in South Africa when spalling was observed within diametrical opposed points of the borehole wall and was oriented in the direction of maximum horizontal stresses. Another early reported case of borehole elongations was made by *Cox* [1970], who observed numerous, uniformly oriented diametrical elongations in 17 oil wells in Alberta, Canada. This was followed by the work of *Babcock* [1978] who established the term borehole breakouts but who concluded that breakouts were controlled by a pre-existing NW-SE joint set which was intersected by the boreholes, and not related to the contemporary stress field. Shortly after this paper, *Bell and Gough* [1979] offered the first theoretical explanation of borehole breakout occurrence, by using the theory of *Kirsch* [1898]. Thereafter, numerous studies [e.g. *Gough and Bell*, 1982; *Hickman et al.* 1985; *Plumb and Hickman,* 1985; *Bell*, 1990] have confirmed that elongations of the borehole cross-sections termed borehole breakouts are a stress related feature. Also several authors have used the observation of borehole breakouts in vertical boreholes to define the orientation of the horizontal principal stresses in many parts of the world [e.g., *Bell and Gough,* 1979; *Zoback* and *Zoback*, 1980, 1991; *Zoback et al.* 1985; *Barton et al.* 1988]. For example, borehole breakout methods were used extensively to determine the orientation of horizontal in situ stresses in the World Stress Map project [*Zoback*, 1992] and the North Sea [*Cowgill et al*, 1993]. As at the year 2003, almost 19% of stress orientation indicators in the WSM database have been determined from borehole breakouts [*Reinecker et al.* 1992].

3.2 Theory of breakouts

Borehole breakouts are zones of failure of the borehole wall that form asymmetrically at the azimuth of the least principal stresses *[Bell and Gough,* 1979; *Zoback et al.* 1985].
When a borehole is being drilled in a homogeneous body experiencing a homogeneous stress field, stresses tend to concentrate around the borehole, since no force can be carried through the interior void. The elastic stress concentration around a borehole drilled along a principal stress axis is described by the Kirsch equations [*Kirsch,* 1898] and subsequently by *Jaegar* and *Cook* [1969] as described in the following equations:

$$\sigma_r = \frac{(\sigma_H + \sigma_h)}{2}\cdot\left(1-\frac{R^2}{r^2}\right)+\frac{(\sigma_H - \sigma_h)}{2}\cdot\left(1-4\cdot\frac{R^2}{r^2}+3\cdot\frac{R^4}{r^4}\right)\cdot\cos 2\theta+(P_b - P_o)\cdot\frac{R^2}{r^2} \quad \text{.....(1)}$$

$$\sigma_\theta = \frac{(\sigma_H + \sigma_h)}{2}\cdot\left(1+\frac{R^2}{r^2}\right)-\frac{(\sigma_H - \sigma_h)}{2}\cdot\left(1+3\cdot\frac{R^4}{r^4}\right)\cdot\cos 2\theta-(P_b - P_o)\cdot\frac{R^2}{r^2} \quad \text{.....(2)}$$

$$\tau_{r\theta} = -\frac{(\sigma_H + \sigma_h)}{2}\cdot\left(1+2\cdot\frac{R^2}{r^2}-3\cdot\frac{R^4}{r^4}\right)\cdot\sin 2\theta \quad \text{.....(3)}$$

where σ_H and σ_h are the maximum and minimum horizontal stresses, R is the borehole radius, r the radial distance to the measurement point, θ is the angle from σ_H, P_b is the

borehole fluid pressure, and P_0 the formation pore pressure. At the borehole wall, $r = R$, and the formulas reduce to:

$$\sigma_r = \Delta P \quad (4)$$

$$\sigma_\theta = (\sigma_H + \sigma_h) - 2 \cdot (\sigma_H - \sigma_h) \cdot \cos 2\theta - \Delta P \quad (5)$$

$$\tau_{r\theta} = 0 \quad (6)$$

Equation 5 and Figure 3 show that the maximum and minimum horizontal stress concentration at the borehole wall occurs at θ = 90º and θ = 0º, respectively.

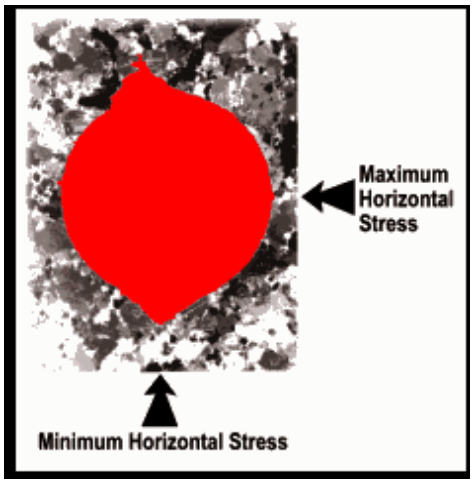

Figure 3: The laboratory experiment of a borehole breakout in a granite rock [see http://www.hydrofrac.com/hfb_home.html **]. Note that maximum and minimum horizontal stress concentration at the borehole wall occurs at θ = 90º and 0º, respectively.**

3.3 Logging tools.

As I earlier mentioned, borehole breakouts are usually identified using four-arm caliper tool, formation microscanner/microimager, and borehole televiewer (Section 1.0). BHTV and FMS/FMI are the most common types of imaging tools [*Meyer*, 2001].

Four-arm caliper tools are designed to measure stratigraphic depression, by depth, correlating formation resistivity measured on four orthogonal pads that are pushed against the borehole wall [*Plumb and Hickman,* 1985; *Meyer,* 2001]. The raw data recorded include: (1) pad one azimuth; (2) borehole deviation; (3) borehole azimuth; (4) the distance between pad one and three (Pad 1-3); (5) the distance between pad two and four (pad 2-4); and (6) the formation resistivity measured by each pad [*Meyer*, 2001]. The reference pad (pad 1) is magnetically oriented to ensure that all orientations are corrected for magnetic declination. Pad 1-3 and pad 2-4 measure the borehole diameter in two orthogonal directions. The four-arm caliper is typically lowered to the base of the borehole and data are recorded while the tool is pulled out back up the borehole [*Meyer*, 2001]. The tool typically rotates, as it is pulled up the borehole due to cable torque. When the tool reaches a zone of borehole breakout, in which tool is ovalised, one pair of pads may become stuck in the borehole breakout. Borehole breakouts can thus be interpreted

from raw dipmeter logs, where rotation is observed below and above the borehole breakout zone and rotation ceases within it [*Meyer*, 2001].

The formation microscanner and – microimager tools (FMS and FMI) are advanced four-arm caliper tools or simply evolved from the dipmeter tool [*Brudy and Kjørholt*, 2001; *Meyer*, 2001]. The tool consists of an array of small electrodes located in each pad, resulting in that a significant area of the borehole wall is being covered during logging [*Brudy and Kjørholt*, 2001; *Meyer*, 2001]. The area of small electrodes on the FMI tool is about twice that of the FMS tool. These electrodes are kept at a constant potential with respect to a return electrode and further up in the borehole. The electrical current emitted by the passively focused electrode is a measure of shallow electrical resistivity in front of the electrode [*Brudy and Kjørholt*, 2001]. The images recorded by FMS/FMI tools depict fine structural bedding planes and thin natural structure as well as borehole breakouts if they are characterized by a resistivity contrast with respect to rock matrix [*Brudy and Kjørholt*, 2001]. .

However, in this study, BHTV and BIPS data were used to detect borehole breakouts. Below follows a more detailed presentation of these tools

3.3.1 Borehole Televiewer (BHTV)

The BHTV is an ultrasonic logging instrument that provides vertically and azimuthally, high-resolution information on the geometrical shape of the borehole and the acoustical reflectivity of the borehole wall [e.g. *Huber et al. 1*997]. The BHTV sonde used by SKB is a High Resolution Acoustic Televiewer (HiRAT). It uses a fixed acoustic source to acquire 2-way travel-time and amplitude of the acoustic signal reflected back to the transducer from a spiral trajectory on the borehole wall. The pitch of the spiral depends on the logging speed and rotating velocity of the mirror. The speed of logging was 2.3 m/min in borehole KFM01B and 2.4 m/min in borehole KFM02A [*Nielsen and Ringgard* [2004a, b]. The start of each spiral is referred to magnetic North during acquisition, using data from the 3-axis magnetometer accelerometer unit in the sonde. The wave train of the reflected signal from the borehole is transmitted to the surface in analogue where it is digitized to real-time. [e.g. *Huber et al.* 1997]. The resulting information is travel-time and amplitude of the pulse reflected off the borehole wall. The oriented data, amplitude and travel-time converted to radius, are displayed as a function of depth and azimuth as unwrapped images of the reflectivity of the borehole wall and provide the exact shape characteristics of borehole breakouts [e.g. *Huber et al. 1*997].

RAMBØLL carried out the BHTV measurements in both boreholes KFM01B and KFM02A using a centralized High Resolution Acoustic Televiewer from Robertson Geologging Ltd, RG 25 112 000 HiRAT [*Nielsen and Ringgard*, 2004], see Table 1 and Figure 4.

Table 1: Parameters recorded by Robertson Geologging Ltd, RG 25 112 000 HiRAT [Lifted from *Ask and Ask*, 2007].

. CALIPER 3D	CALIPER 3D is calculated using both variables of the acoustic travel time and the velocity in the borehole fluid. The velocity in the fluid is calculated using the fluid temperature and fluid conductivity *[Nielsen and Ringaard,* 2003; 2004].
CALIPER MEAN	CALIPER MEAN is calculated using the mean travel time from the acoustical televiewer, the fluid temperature, fluid velocity and the internal travel time in the acoustical televiewer;
Travel Time	TRAVEL TIME is a 360º oriented travel time image represented in gray scale. Travel time units are 0.1µs, and reveals the borehole diameter provided if an estimate of the acoustic velocity in the borehole fluid is available.
Amplitude	AMPLITUDE is a 360º oriented amplitude image in color scale. Amplitude is dimensionless, reveals the acoustic impedance of the borehole wall that is related to geotechnical rock properties;
Azimuth	AZIMUTH is the orientation of the tool with respect to magnetic North (0-360ºN). The data have been corrected for magnetic declination.
Dip	DIP is the borehole inclination from the horizontal and it varies from 0-90º. The Dip reveals the orientation of the tool within the borehole, which may not follow the orientation of the borehole, because of the smaller probe diameter (45 mm) relative to the borehole diameter (76 mm).

Figure 4 High Resolution Acoustic probe RG 112 000 HiRAT that was used to log boreholes KFM01B and KFM02A.

3.3.2 Borehole image processing system (BIPS)

The Borehole image processing system (BIPS) produces a digital scan of the borehole wall. A standard computer controlled digital (CCD) video camera is installed in the probe in front of a conical mirror. An acrylic window covers the mirror part, and the borehole image is reflected through the window part and displayed on the cone, from where it is recorded [*Nilsson and Gustafsson*, 2003; *Gustafsson and Gustafsson*, 2004], see Figure 5. Boreholes KFM01B and KFM02A were both logged with a radial resolution of 360 pixels/circle and a vertical resolution of 1mm on a magneto optical disc (MO-disc) in the surface unit. The maximum speed during data collection was 1.5 m/min [*Nilsson and Gustafsson*, 2003; *Gustafsson and Gustafsson*, 2004]. A gravity sensor was used to

measure the orientation of the BIPS image, and the orientation of the tool was manually recorded during logging. This result in that BIPS images are not re-oriented versus North; rather, the images are shown with respect to the tool orientation (D, L, U, R, i.e. down-, left-, up-, right-side of the tool, respectively.

RAYCON carried out BIPS measurement in boreholes KFM01B and KFM02A using the BIPS 1500 system.

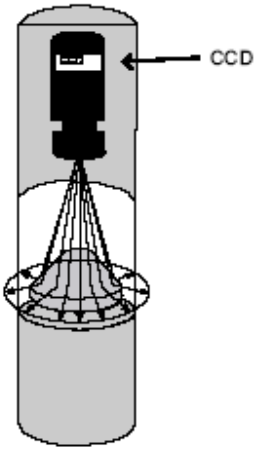

Figure 5: The conical mirror scanning in the BIPS system [After *Gustafsson* and *Gustafsson*, 2004]

3.4 Analysis

3.4.1 Borehole breakout analyzing program

During this project, SKB has provided two computer programs for analyzing logging data: - WellCAD Readers (version 4.0 build 729), and BIPS image viewers for Windows 95/NT (version 2.51). The former was used to view BHTV images whereas the later was used to view the BIPS data. Table 2 shows the list of data files that were used to analyze borehole breakouts in both boreholes (KFM01B and KFM02A). The data file were provided by SKB and delivered as SICADA_06_134_1.

Table 2: The list of data files sent for analyses of borehole breakouts sent by the SKB database SICADA (delivery Sicada_06_134_1)

Borehole	Name of data file	Data type
KFM01B	KFM01B_Presentation.WCL KFM01B_KFM01B_SwedPower_D_bdt	Geophysical loging data including BHTV, caliper-1, density, resistivity, etc. BIPS data including structural interpretations.
KFM02A	KFM02A_Presentation.WCL KFM02A_HIRAT_up_120_run2. LGX KFM02A_KFM02A_SwedPoweer_tot.bdt	

3.4.1.1 WellCAD (Version 4.0 build 729)

WellCAD is a PC program designed by Advanced Logic Technology [©Advanced Logic Technology (ALT)]. This program contains the BHTV log. The amplitude image was plotted as a function of azimuth and depth thereby enabling breakouts and other borehole related features to be detected. The data file listed in Table 2 was imported into this program. Readings are made in two different ways i.e. by using a static and a dynamic plot of the amplitude log. The basic difference between the plots is that the dynamic plot has its color palette and scale altered for a better distinct view of borehole breakout points whereas the static plot has fixed colors but with a change in scale The normalization of the dynamic and static logs provides complementary images of structures, both geological and drilling related structures. Furthermore, the depth scale in static color scale was 1:500 m but was modified to 1:10 m in dynamic color scale. By modifying the depth scale, a borehole breakout could be viewed at a wider range. Most of the analysis was actualized using the unwrapped amplitude log but in most cases comparison was made with the travel-time log and stacked Caliper 3D log which gives a view of geometry of the borehole from plotting cross-section of the 3D caliper data.

3.4.1.2 BIPS Image Viewer for Windows 95/ NT, version 2.51

I have used the BIPS image viewer to confirm or reject borehole breakout sections that have been identified in the BHTV image data. This is to say that the majority of breakouts identified were mainly with BHTV image. The BIPS images from SKB boreholes have known limitations: For example, *Berglund et al.* [2004] pointed out four limitations for BIPS images.

1) BIPS images are associated with poor resolution due to presence of suspended cuttings in the borehole fluid;
2) It is very difficult to distinguish a thin fracture sealed by low contrast mineral;
3) Oxidation of some sort has taken place in many SKB boreholes, and BIPS images do not view the underlying fresh rock; and lastly
4) It is difficult to distinguish infilling minerals such as laumonite in BIPS images.

In addition, *Ask and Ask,* [2007] argued that borehole breakouts could only be observed in BIPS images in distinct breakout zones or if clear fractures have been formed. More so, that borehole breakouts in amphibolites often revealed light reflections on individual grains, so that reflections could be observed in diametrical sides of the borehole.

3.4.1.3 Microsoft® Excel 2000

Microsoft Excel has mainly been used for making tables and analyzing data. The tables included records of borehole breakout data. For each borehole breakout zone, the depth, orientation of the top, bottom and mean, the type of breakouts and their degree of clarity were recorded (Tables 9 and Table 10). Figure 6 shows how these parameters were picked for a borehole breakout zone. The data analyses included calculations of the average orientation of borehole breakouts and their standard deviation. According to the WSM criteria (Section 3.4.4 and 3.4.5) [*Zoback, 1992*], the individual lengths of borehole breakout zones were taken into account for calculating the mean orientation and standard deviation. The mean orientation of borehole breakouts (θm) of a population of n-picked borehole breakout direction (θi), is derived by first transforming the angles to the θ-360º

interval (i.e., θ-2θi) [*Mardia*, 1972; *Reinecker et al*., 2003]. Then, the direction cosine and sine have to be added and averaged by the total borehole breakout length (i.e., length weighted mean) according to equations 7 – 11:

$$L = \sum_{i=1}^{n} li \quad \text{.....(7)}$$

$$\cos \theta i = \frac{1}{L} \sum_{i=1}^{n} li \cos \theta i \quad \text{.....(8)}$$

$$Sin \theta i = \frac{1}{L} \sum_{i=1}^{n} li \sin \theta i \quad \text{.....(9)}$$

$$\theta m = \tfrac{1}{2} \arctan\left(\sin \theta i \,/\, \cos \theta i\right) \quad \text{.....(10)}$$

$$So = {}^{360}\!/_{2\pi} \left(-\tfrac{1}{2} \log eR\right)^{\frac{1}{2}} \quad \text{.....(11)}$$

Note: $R = \left(\sin \theta i^2 + \cos \theta i^2\right)^{\frac{1}{2}}$

Where, li and θi are the length and orientation of borehole breakout intervals, respectively. θm is the mean breakout azimuth, So is the standard deviation.

3.4.1.4 KaleidaGraph 4.03

The Kaleidagraph 4.03 is a graphical plotting and statistical program [©Synergy Software]. I mainly used this program to make scatter plots of borehole breakout lengths versus mean orientation of borehole breakouts (Figure 20 and Figure 24). Section 3.4.2 and Figure 6 illustrate how these parameters are picked for a borehole breakout zone.

3.4.2 Data Analysis

A detailed analysis of BHTV data precisely measures the borehole shape with depth [*Barton et al*. 1997]. Borehole breakouts appear as dark bands of low reflectance on opposite sides of the borehole wall. They are identified as diametrically opposed pairs of bands with high travel-time and low amplitude, parallel to the borehole axis on the BHTV amplitude/travel-time log (Figure 6). While in some cases, borehole breakouts are found to run along the borehole length as a single feature, i.e., occurring in one side of the borehole wall (single borehole breakout). The minimum width of a borehole breakout is a function of initial failure of the borehole wall upon breakout formation [*Zoback et al*. 1985]. The two pairs of radial lines are used to define the edges of borehole breakouts (Figure 6). The width is the difference in these azimuths. Since the azimuth of borehole breakouts does not often form symmetrically, then it becomes imperative to save these values independently for each side of the borehole.

In computing the breakout data, readings are made by taking note of the depth scale and orientation at which borehole breakouts were formed by registering the top, bottom and the mean of the borehole breakout interval (see Table 9, Table 10 and Figure 6). The mean borehole breakout was determined by taking the average of the top and bottom

depth of the borehole breakout interval. The type of borehole breakout was reviewed in two different ways; registered as single when it is formed at only one side of the borehole wall (see Figure 22 and Figure 26) or diametrical when it is formed at both sides of the borehole or ±180º apart (see Figure 21 and Figure 25). Their degree of clarity was recorded also on three different scales of sharp, medium and low based on how deep, shallow, visible and well pronounced the borehole breakout appears (Table 9 and Table 10). However, the majority of borehole breakouts observed in both boreholes analyzed are shallow; it is therefore not too common to observe borehole breakouts that have a high degree of clarity.

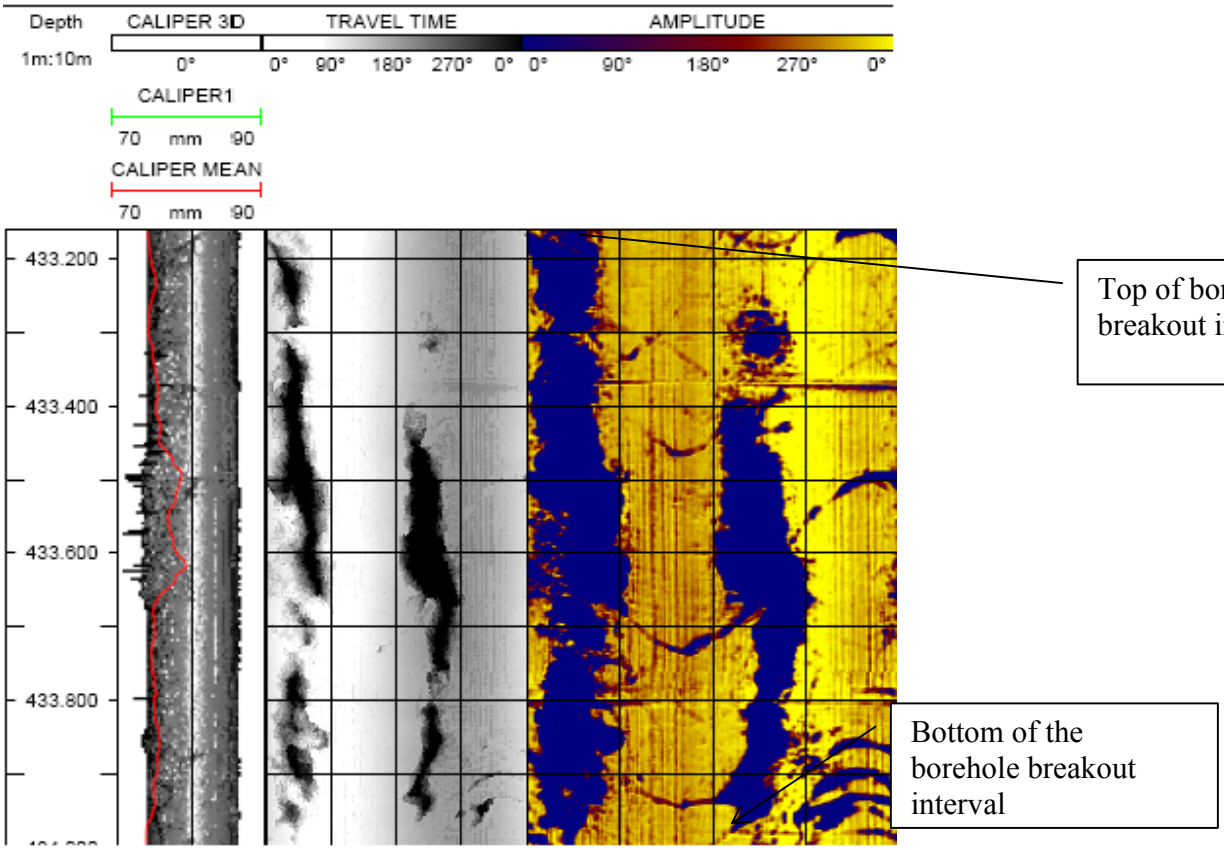

Figure 6: Example of diametrical borehole breakout identified in borehole KFM01B at the Forsmark site. Note that the figure indicated the top and the bottom of the borehole breakout.

3.4.3 Criteria for analyzing borehole breakouts

The criteria for analyzing borehole breakouts were initially proposed by *Plumb and Hickman* [1985]. The authors examined the validity of using the four-arm dipmeter to identify borehole breakouts. They logged a well in Auburn, New York, twice with a four-arm dipmeter and once with a borehole televiewer. Subsequently, they compared the orientation of borehole breakouts from the four-arm dipmeter with borehole cross-sections constructed from BHTV data. They found that the four-arm dipmeter generally had its long axes aligned with the borehole breakouts. This was a critical observation as most of the boreholes logged before with four-arm dipmeter lacked detailed BHTV observations. These observations led *Plumb and Hickman* [1985] to propose the initial

criteria applied for identifying borehole breakouts using four arm caliper tool. However, in this project or research work, I used a set of criteria proposed by *Reinecker et al*. [2003] as a guide. *Reinecker et al*. [2003] is a member of the WSM project. The author combined several criteria proposed by prominent authors [e.g. *Plumb* and *Hickman*, 1985; *Bell,* 1990; *Zojack* and *Stock*, 1997] by using the four-arm caliper tool and came up with the criteria listed in Table 3.

The initial two and the fourth criteria relate to rotation of the dipmeter due to torque as the tool is winched up the borehole. The first and the second criteria require the dipmeter to track the borehole breakout, and the third criterion eliminates position where the dipmeter is not centered in the borehole or where the borehole is washed-out. The fourth criterion deals with the observation that a caliper difference less than 10% of the bit size is sufficient enough to stop tool rotation for the *Reinecker et al.* [2003] winch cable set up. The fifth criterion addresses cable and tool drag on the borehole wall and creates a channel of the low side of the borehole (keyseat) yielding to a roughly elliptical borehole shape that could be interpreted as a borehole breakout if only caliper data were available. The last criterion addresses the fact that borehole breakouts shorter than the length of the caliper pads cannot be measured since the dipmeter referred to here is assumed to have pads of about 1 m length.

Table 3: Criteria for interpreting borehole breakouts based on four-am caliper data by *Reinecker et* al. [2003].

1. Tool rotation must cease in the zone of enlargements.
2. There must be clear tool rotation into and out of the enlargement zone.
3. The smaller caliper reading is close to bit size. Top and bottom of the breakout should be properly marked.
4. Caliper difference has to exceed bit size by 10%.
5. The enlargement orientation should not coincide with the high side of the borehole in wells that deviated by more than 5º.
6. The length of the enlargement zone must be greater than 1 m.

The boreholes in this study were logged using the BHTV tool. The BHTV tool have a higher resolution than the four-arm caliper tool and therefore could be able to detect much smaller borehole breakout depths which ordinarily could not be detected with four-arm caliper tools as a result of its pad geometry.

Table 4: Criteria for identifying borehole breakouts from BHTV data

1. The top and bottom of the breakout should be clearly marked, by a distinct color change in travel time and/or amplitude images.
2. Two clearly discernible borehole elongations (i.e., low or even zero amplitude and highly increased radii) with necessary 180º spacing in unwrapped amplitude. Offset with depth of $\leq$ 0.5 m is acceptable between the two grooves.
3. The length of borehole breakouts should be $\geq$ 0.5 m.
4. The mean angle of a breakout is picked based on the orientation of a borehole breakout determined at the central width of the entire borehole breakout.

5. If a single groove has similar physical appearance and orientation as the parallel grooves of individual borehole breakouts, it is assumed that the diametrical trace has not yet developed or that artifacts from logging or processing even out the second grooves.

The initial criterion required the top and bottom of borehole breakouts to be marked, thus enabling to obtain the mean orientation of borehole breakouts and also the span (extent of occurrence).

The second criterion addresses the fact that though the borehole breakout is separated by 180º apart, still most of the borehole breakouts do not start and end at the same depth interval. Therefore, it is deemed necessary to give room for an offset with a depth of ≤ 0.5 m between the two borehole breakout grooves (note this is only applicable to diametrical borehole breakouts).

The third criterion proposed a borehole breakout length of about 0.5 m unlike when using a four-arm caliper tool that proposed that the length of the enlargement zone must be greater than 1 m (see Table 3 and also the second to the last explanation after the table).
The fourth criterion suggested that the orientation of borehole breakouts is determined at the central width of the entire borehole breakout, which is obtained from the average value of the maximum azimuth of the breakout.

Lastly, the fifth criterion was included due to the fact that several single borehole breakouts were identified in both boreholes studied. This was possible due to the similarity between single and individual traces of diametrical borehole breakouts. Since both have similar orientation and physical appearance it therefore seems necessary to include it in this present study. More so, it was observed that most of the studies previously carried out with four-arm caliper tool lack detailed single borehole breakout observations.

3.4.4 Statistical analysis

In order to determine the orientation of the stress field, the mean σ_H-orientations for the two boreholes were analysed using a length weighted mean. This may simply suggest that individual borehole breakouts were weighted by its own length to enhance the dominant σ_H-orientation. Consequently, the orientation and standard deviation (std. dev) were calculated for each borehole to rank them according to the World Stress Ranking Scheme (WSM). This was achieved using Microsoft excel as previously discussed in Section 3.4.1

3.4.5 World Stress Map (WSM) Quality Ranking Scheme

All borehole breakout stress indicators compiled in this thesis have been quality ranked according to the WSM ranking Scheme [*Zoback,* 1992]. The quality ranking for borehole breakouts is based on standard deviation (s.d.), and number and/or length of breakout zones. In addition, certain numbers of breakout zones must be attained. Table 5 presented the World Stress Map quality ranking according to *Zoback* [1992]. The author suggested that for a single borehole, that A>B>C>D and E.

Table 5: The World Stress Map Quality Ranking for borehole breakouts [*Zoback*,1992].

Borehole breakouts	Ranking Quality
≥ 10 borehole breakout zones with an s.d. ≤ 12º and/or a combined length > 300m;	A-quality
≥ 6 borehole breakout zones with an s.d. ≤ 20º and/or a combined length > 100m;	B-quality
≥ 4 borehole breakout zones with an s.d. ≤ 25º and/or a combined length	C-quality
≥ 4 borehole breakout zones with an s.d. ≥ 25º and a combined length < 30m;	D-quality
Boreholes in which no reliable breakouts are detected, alternatively with an extreme scatter of orientations and no significant mean (s.d. > 40º)	E-quality

Zoback [1992] considers A- to C- quality data to be significant indicators of the tectonic stress field, while D and E-qualities give vital information about the local state of the stress and/or variations in the mechanical properties of the sediment.

3.5 Quality of data

The possibility of identifying breakouts or other borehole related elongations in both boreholes are strictly dependent on the quality of the image tool used in this analysis. This section will focus mainly on the data quality problems associated with the BHTV log. The majority of the identified breakouts in this study are mainly influenced by data quality. The quality of BHTV data was influenced by drilling as well as artifacts that have been introduced during logging and/or subsequent data processing. *Lofts and Burke* [1999] provided a detail summary of logging artifacts, which are presented in detail below. Identified artifacts include:

1) Drilling induced spiral grooves in the borehole wall;
2) Keyseat;
3) Washouts and lastly;
4) Sticky zones

The drilling artifacts were more numerous in borehole KFM02A compared to borehole KFM01B. Few sections were affected in borehole KFM01B whereas almost 41% of the entire borehole length was affected in borehole KFM02A (this value is only for spiral grooves).

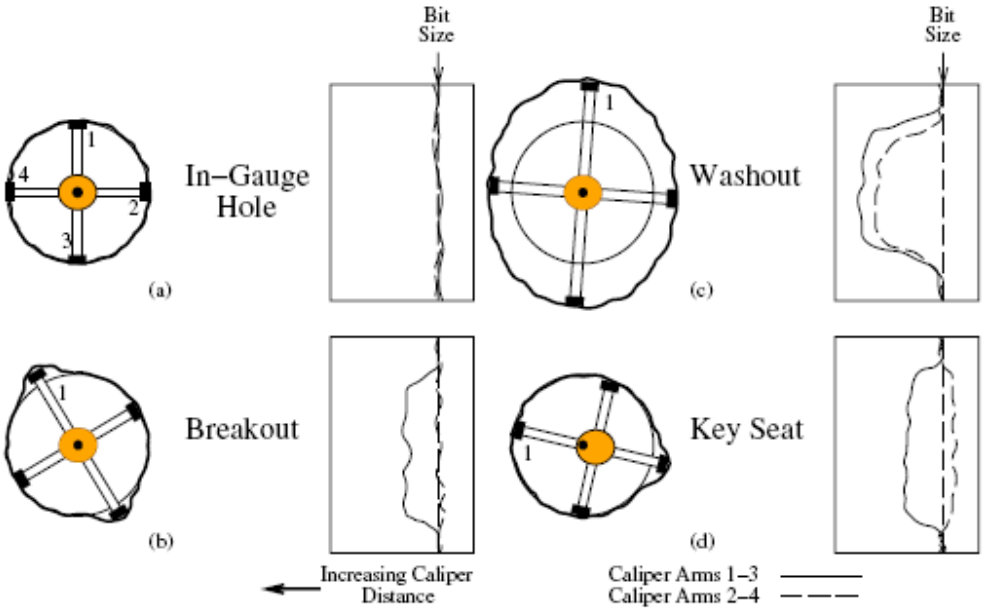

Figure 7: Common types of enlarged borehole and their caliper log response [lifted from P*lumb and Hickman,* 1985]

3.5.1 Spiral grooves

Drilling induced grooves (see Figure 8) usually appear when the borehole wall is grooved due to scratching by the bit and often associated with a mild to thick diagonal mark on the BHTV log [*Lofts and Bourke*, 1999].

Figure 8: Example of spiral grooves [After Lofts and Bourke, 1999]. Note that spiral grooves may form thick diagonal marks or grooves that run across the BHTV amplitude log.

3.5.2 Keyseats

Keyseats (see Figure 9) result from ovalisation due to bit wear on the underside of the borehole, which is commonly observed in inclined boreholes [*Lofts and Bourke.* 1999]. More so, it can result from a large feed force during drilling. Keyseats are identified as a low reflective band in either the high or the low side of the borehole in BHTV log, especially in an inclined borehole.

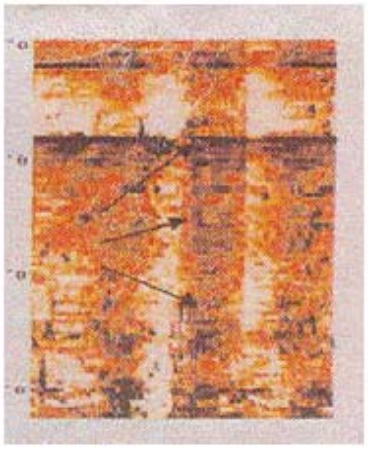

Figure 9: Example of keyseats [After Lofts and Bourke, 1999]

3.5.3 Washouts

Washouts (see Figure 10) are enlargement of the borehole diameter and corresponding defocusing of image. Washouts are identified as dark and patchy images on the BHTV log and can have a severe effect on this log *[Lofts and Bourke,* 1999].

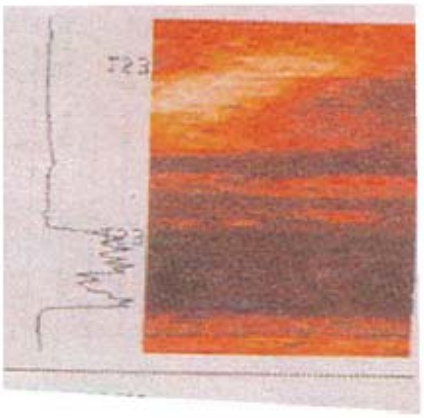

Figure 10: Example of a washout zones [After Lofts and Bourke, 1999]. Washout zones are the dark/patchy images on the BHTV amplitude log

3.5.4 Sticky zones

Sticky zones occur as a result of tool motion being erratic or jerky. Sticky zones can be identified as blocky patches on the BHTV log [*lofts and Bourke,* 1999], see Figure 11.

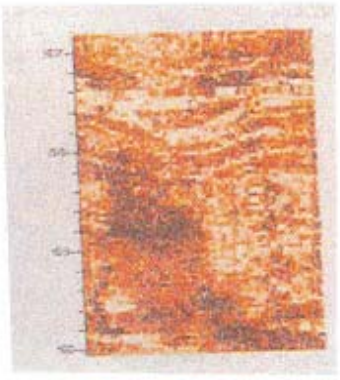

Figure 11: Example of sticky zone [*After Lofts and Bourke*, 1999]. Note that sticky zones are the blocky patches on the BHTV amplitude log.

4.0 DRILLING AND MWD DATA

4.1 Introduction

Drilling is one of the most important activities carried out within the scope of Forsmark site investigation programme. The drilling programme enables SKB to achieve the following objectives [*e.g. SKB, 2000]*:

- To have information on the penetrated soil and rock volume by recording drilling and flushing water parameters through the observations of the drilling process documented by the drilling personnel;
- Enables the material (drill core, drill cuttings and groundwater) from different depth to be brought to the surface so that the studies from various aspects could be achieved;
- Serves as an opportunity to lower different types of measuring instruments into the hole after drilling, whereby geoscientific parameters can be determined at different levels;
- Enables to compile and evaluate data from drilling and MWD whereby the knowledge of the site's geological character and ground water conditions could be ascertained.

Borehole KFM02A is drilled using telescopic drilling technique [*Claesson et al*. 2004; 2005]. This technique comprises both percussion drilling and core drilling. Percussion drilling technique enables the first 100 m of the borehole to be drilled with In The Hole (ITH) technique. In this particular technique, compressed air is used as a flushing fluid, to drive the hammer, and as well to transport the cuttings to the surface. The advantage of conventional percussion drilling is that the method produces boreholes quickly and cheaply compared with core drilling. However, the limitation of this technique is that the information on rock type and fracture distribution that can be obtained directly from drilling is more limited [*SKB 2004*]. After completed percussion drilling, the borehole section 0-100 m was cased and the gap between the casing and the borehole wall was grouted.

The rest of the hole, after the first 100 m was drilled with core drilling, that is rotary drilling with an annular, diamond-typed bit. As the drill works its way downward, a cylindrical core is produced. The drill bit is followed by a core barrel, which is gradually filled up by the core as drilling proceeds. When the core barrel, which is generally 3 m, 4.5 m, or 6 m long-is full, it is brought to the surface and its content emptied.

Borehole KFM01B is conventional core drilled borehole, i.e., core drilling started immediately from the surface. The section through the soil layer is cased.

4.2 Measurement While Drilling (MWD)

Measurement while drilling entails recording of drilling parameters during the drilling process. MWD data were only recorded for borehole KFM02A. The measured parameters are listed in Table 6. Measured drilling parameters are used for judging the progress of the drilling work in a pure technical sense but may also be of geoscientific

interest, since they can either directly or indirectly reflect the properties of the drilled rock formation. For example, drilling rate depicts the speed with which the drill-bit moves through the rock. Therefore, drilling rate is a function of rock properties such as hardness and fracture contents, but it is also dependent on feed pressure, rotary speed and drill-bit condition. The information acquired from measuring and analyzing the drill rate could give a basic knowledge about the rock at depth. Borehole KFM02A was drilled using an ONRAM 2000-CCD (Computer Controlled Drilling) drilling machine. The ONRAM hydraulic driving device is incorporated with an in-built transmitter that provides input in form of signals to a trigger unit thereby enabling specific software to control the drilling operation [*Claesson and Nilsson*, 2004]. Data collections during drilling were achieved via an automated recording system. Because the system for MWD data collection is automatic, it is difficult to draw safe conclusions about the affect of MWD parameters [*Lennart Ekman, Pers. Comm.*, 2008].

4.3 MWD Data Analysis

For the cored part of borehole KFM02A (100.42 – 1002.27 m) filtered data from SKB were used. The borehole was logged at intervals of 1cm but some of the sections listed in Table 6 were missing (Table 6).

Table 6: The missing data sections in borehole KFM02A

1) 139.01 -140.26 mbl;
2) 140.18 – 141.43 mbl;
3) 201.163 – 203.13 mbl;
4) 203.18 – 204.44 mbl;
5) 249.48 – 250.77mbl;
6) 252.59 – 254.09 mbl;
7) 258.22 – 259.44 mbl;
8) 260.33 – 262.23 mbl;
9) 264.65 -266.12 mbl;
10) 267.21 – 268.65 mbl;
11) 268.67 – 270.16 mbl;
12) 279.53 – 281.04 mbl
13) 803.16 – 803.6 mbl;
14) 848.87 – 849.12 mbl;
15) 878.72 – 879.08 mbl.

The original data file sent by SKB was in two files namely: Microsoft Excel-mwd_filtered_data_0.002.xls [Read only] and Microsoft Excel-mwd_filtered_data_0.003.xls [Read only]. The file occupied a total of 25 columns and 75,431 rows that made it impossible to be stored in one Excel work sheet due to Excel size limitation. The parameters in Table 7 were recorded in the MWD data that were sent by SKB.

The parameter ‘‘mode ‘’ represents the current activity in drill cycle, whereas, the drill ‘‘status’’ gives an explanation of the drill stops and also indicates when a drilling sequence is finished. Water flow provides basic information of the hydraulic properties of

the rock [*Shunnesson,* 1999] which includes water carrying fractures or openings, some indication of water flow-in, etc. Furthermore, measuring the rate of penetration or simply feed speed as a function of rotation and thrust or weight of the drill bit enables the relative hardness of the penetrated formation to be described [*Sinkala* 1987*,* also see section 4.2].

In making plots for the correlation between borehole breakouts and MWD parameters, I selected five out of twenty-five parameters recorded in Table 7. These five parameters are assumed to give a clear indication of changes and variations with depth as drilling progresses. The selected parameters include: - rotation pressure (bar), water flow (l/min), water pressure (bar), rotation speed (rpm) and lastly, feed speed (cm/min).

Table 7: The recorded MWD parameters in borehole KFM02A

Activity ID
Activity type
ID code
Sign
Borehole length (m)
Date (day/month/year)
Mode
Status
Rotation pressure (bar)
Feed force drill bit (kg)
Feed force of the cylinder (bar)
Water flow (l/min)
Water pressure (bar)
Rotation speed (rpm)
Feed speed or penetration rate(cm/min)
Drill length (cm)
Drill-bit position (cm)
Feed position (cm)
Rod weight (kg)
Rod pressure (bar)
QC. Ok
Northing
Easting
Elevation
Coordinate system

In selecting borehole breakout points for the plots, a section in the borehole with a deep borehole breakout was picked from the amplitude log and at the same time inferring such intervals with the MWD dataset. Whereas in the sections without borehole breakouts, I avoided major geologic discontinuities like fractures that might interfere with my results,

since borehole breakouts and fractures may be reflected alike in MWD parametric signatory.

5.0 RESULTS

5.1 Logging Artifacts

5.1.1 Spiral grooves

Spiral grooves were identified in several sections in both borehole KFM01B and KFM02A. The three most prominent sections with spiral grooves in borehole KFM01B are from ~ 273-309 mbl; ~393-397 mbl and 458-465.4 mbl whereas those of borehole KFM02A are listed in Table 8. In the latter borehole, spiral grooves occurred along almost 41% (413.7mbl) of the entire borehole length. They occur as diagonal marks that run across the borehole wall and are clearly visible in both BIPS and the BHTV log (Figure 12, Figure 13 and Figure 14. Figure 12 is a BHTV log (image) of the spiral grooves identified from ~ 289-291 m in borehole KFM01B whereas Figure 13 is a BIPS image of spiral grooves identified from ~ 337.9-338.4 mbl in borehole KFM02A. Lastly, Figure 14 shows a BHTV log (image) of spiral grooves identified from ~349-350 mbl in borehole KFM02A. The spiral grooves are so intense (thick) in most of the sections in borehole KFM02A that it was very difficult to have a good view of the entire borehole wall. Also some spiral grooves are combined with washouts while some are combined with borehole breakouts. A typical example is displayed in Figure 29. In the later example, it is very difficult to identify the beginning and the end of the borehole breakout zone. This may result in that some of the borehole breakout zones may be concealed by poor quality of data, which may result to an underestimation of some of the borehole breakout zones.

Table 8: Sections in borehole KFM02A with spiral grooves.

1. 104.76 – 136.56 mbl;
2. 146.96 – 159.34 mbl;
3. 262 – 297 mbl;
4. 338 - 363.98 mbl;
5. 373.74 – 427.60 mbl;
6. 477.25 – 502.80 mbl;
7. 538.51 – 573.25 mbl;
8. 597 - 613 mbl;
9. 666.12 – 692.60 mbl;
10. 721.23 – 748.57 mbl;
11. 872.2 – 921.8 mbl;
12. 923.65 – 930 mbl;
13. 936.7 – 964.2 mbl;
14. 978.4 – 1001.8 mbl.

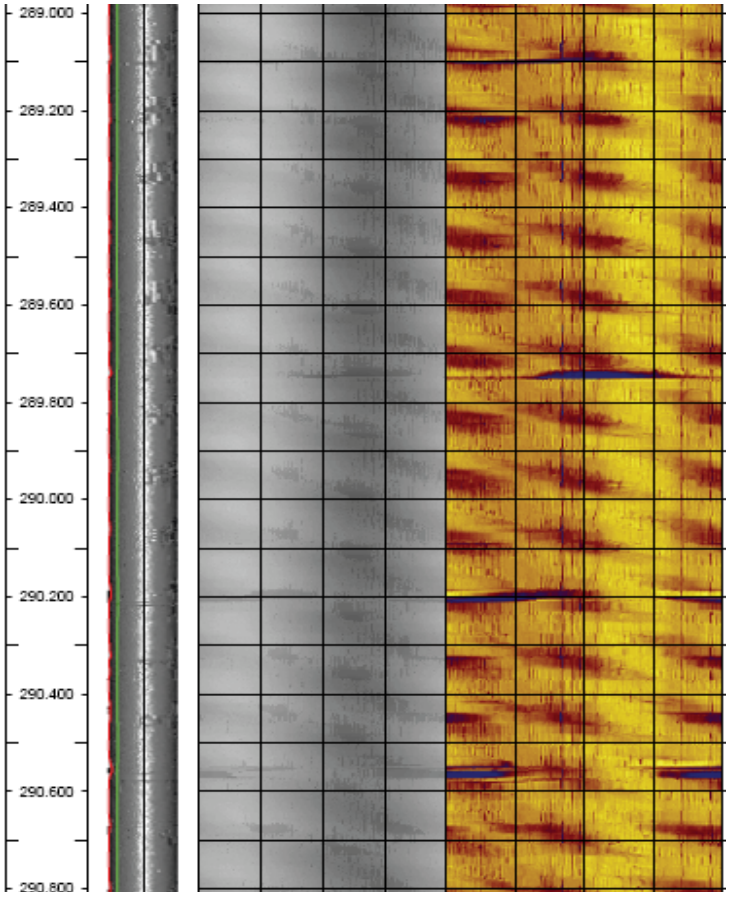

Figure 12: A spiral grooves identified from 289.0-290.8 mbl) in borehole KFM01B. The spiral grooves are the dark diagonal bands that run across the BHTV log. The section with spiral grooves is more often visible in the BHTV amplitude log than in BIPS image.

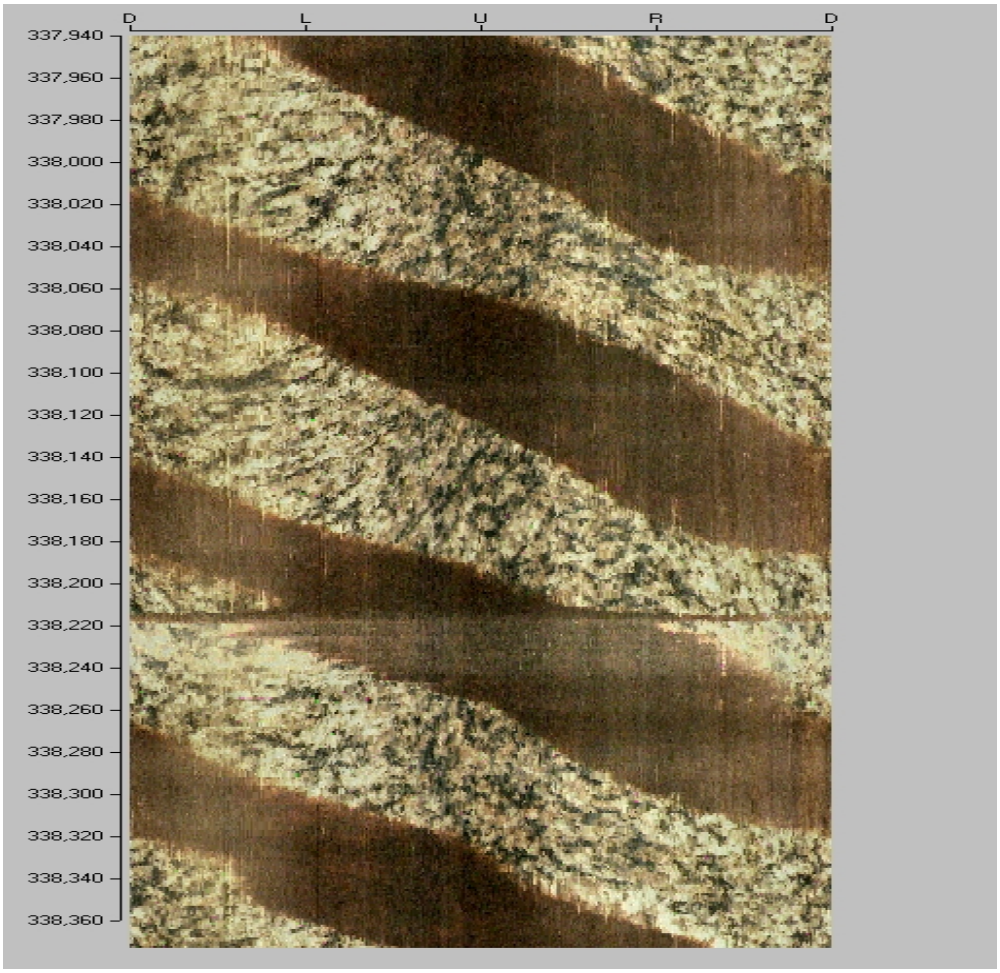

Figure 13: Showing a section (337.94-338.36 mbl) of BIPS image in borehole KFM02A with spiral grooves, which appear as a dark diagonal bands that run across the borehole wall (i.e., across the crystalline rock).

5.1.2 Keyseats

Keyseats were identified in the upper part of borehole KFM01B (~12-62 mbl; Figure 15), where it occurs as a dark reflective band along the azimuth of 264-286˚N, which is sub-parallel to the hole azimuth. In borehole KFM02A, keyseats were identified from about 135 to 159 mbl (Figure 16). They occur as dark reflective bands along azimuth 73-90˚N, which is sub-parallel to the hole azimuth.

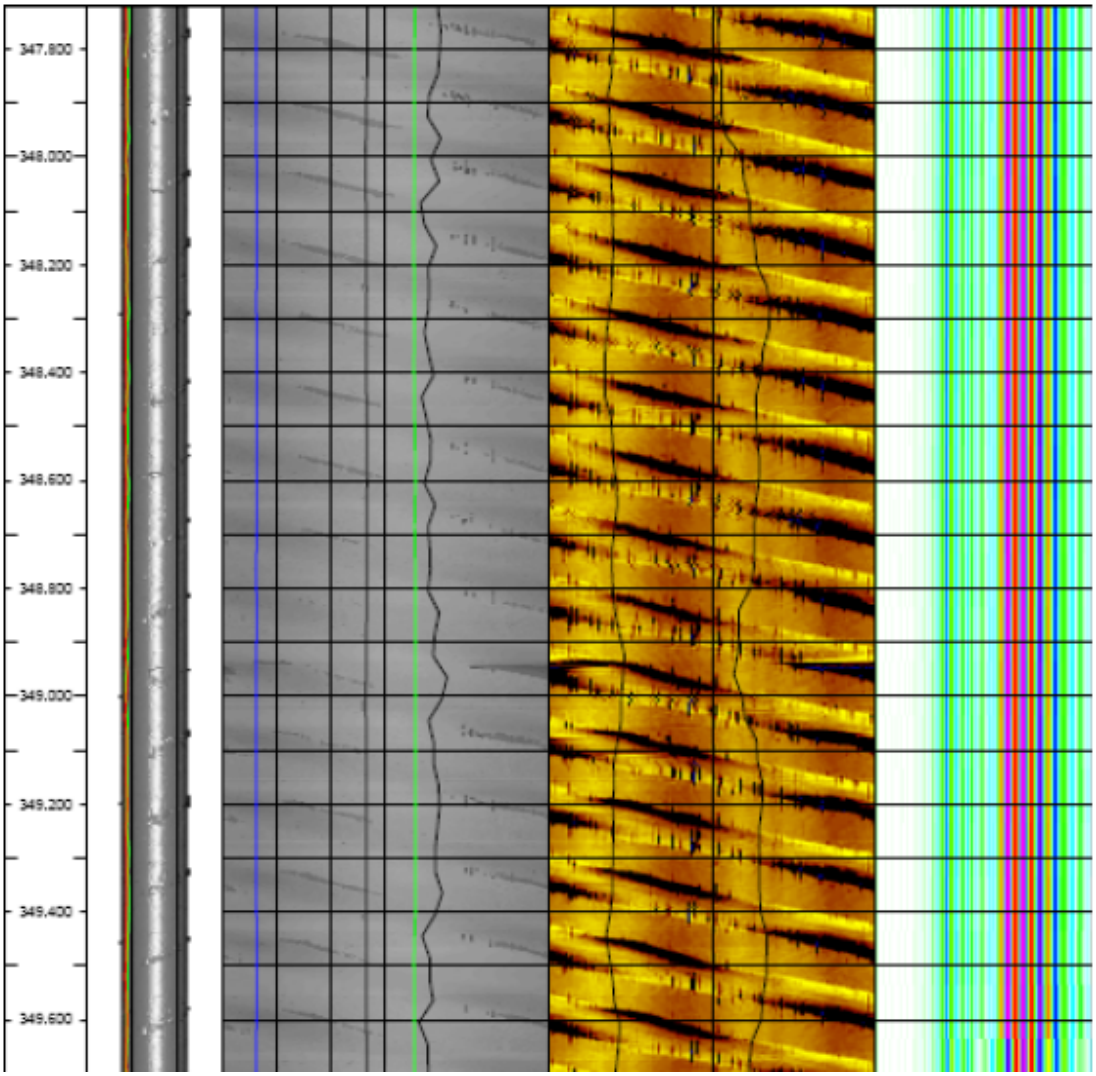

Figure 14: Example of spiral grooves identified from 347.8 – 349.6 mbl in borehole KFM02A. Note that the spiral grooves is so thick that it was visible in three of the BHTV logs (i.e., caliper 3d, traveltime and amplitude log. But the severity was more in the amplitude log.

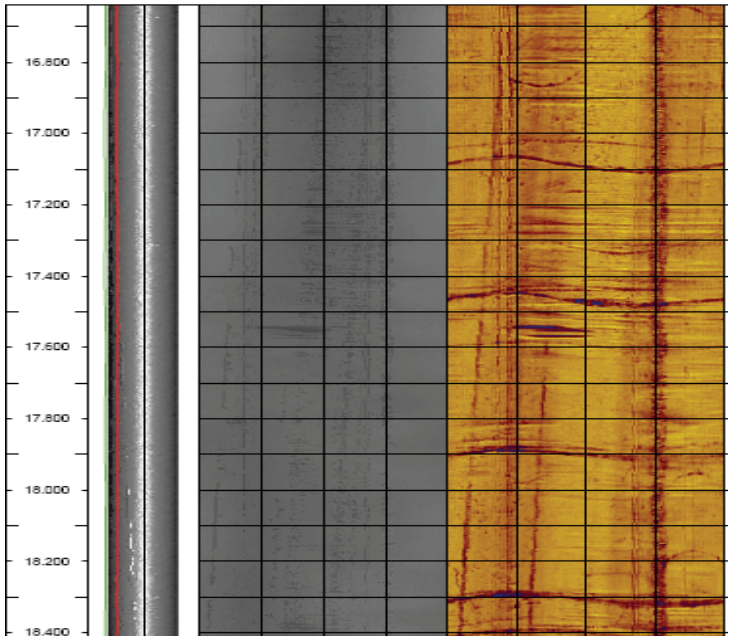

Figure 15: A section (16.7-18.4 mbl) in borehole KFM01B with keyseat. The keyseat was visible in the BHTV amplitude log and has its azimuth from 264º - 284ºN.

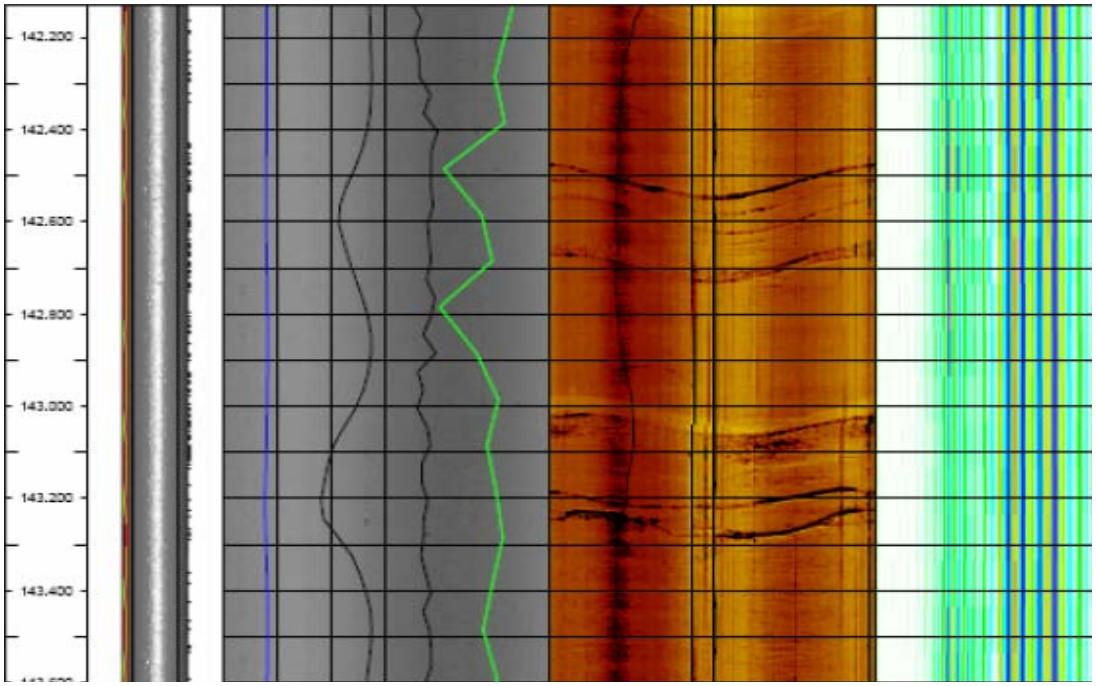

Figure 16: One of the section in borehole (142.2-143.5 mbl) in KFM02A with keyseat. The keyseat was visible in the BHTV amplitude log and has an azimuth from 73-90ºN.

5.1.3 Washouts

Washout zones were rarely observed in borehole KFM01B. The two most prominent sections occur at 48.9-50.5 mbl and 419-420 mbl (Figure 17). In borehole KFM02A, washouts occur at 118.1-119.2 mbl, 119.8-172.2 mbl and 266.5-267.3 mbl, respectively, and were clearly visible in three of the BHTV logs (caliper 3d, traveltime and amplitude log; Figure 5.1.3 (a, b)). It occurs as spikes that envelop almost the entire part of caliper 3d log. But in the traveltime log (middle), washout zones occur as dark deep bands (black) that are more pronounced from ~ 419.15-418.8 mbl in borehole KFM01B and from 118.3- 119.4 mbl in borehole KFM02A, whereas it occurs as deep blue bands that embrace almost the entire amplitude log in Figure 17 and Figure 18).

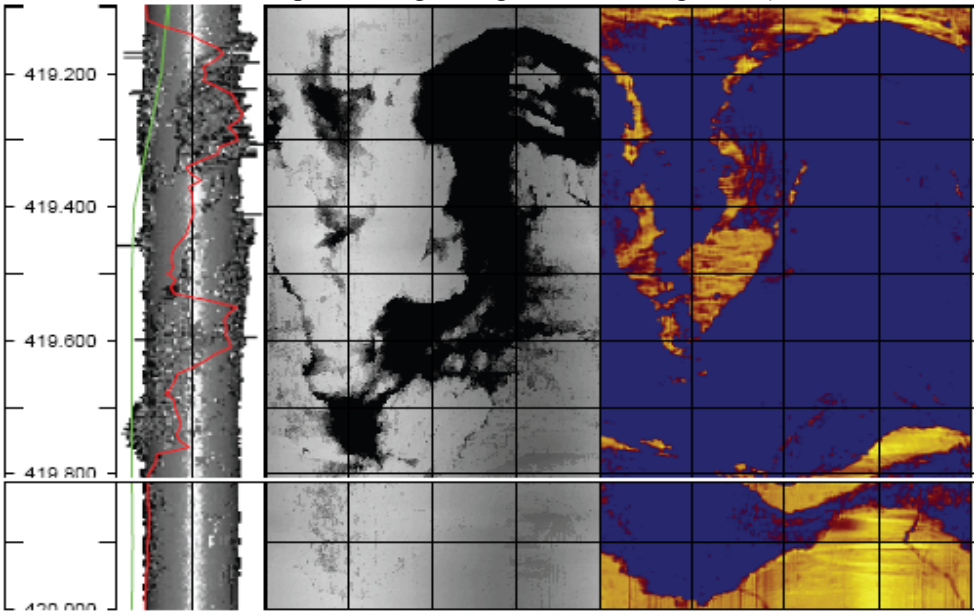

Figure 17: A washout zone (419.0-420.0 mbl) in borehole KFM01B. This zone was clearly visible in three of the BHTV logs (Caliper 3D, travel-time and amplitude log).

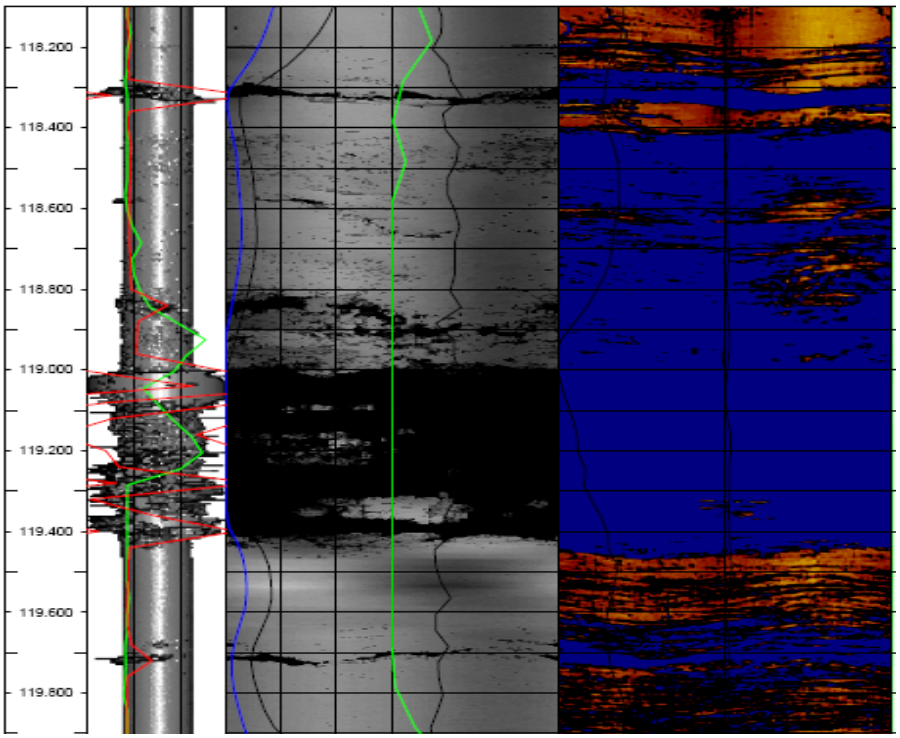

Figure 18: A washout zone (118.1-119.9 mbl) in borehole KFM02A. This zone was clearly visible in three of the BHTV logs (Caliper 3D, travel-time and amplitude log).

5.1.4 Sticky zones

Sticky zones were identified at 135.6-136.8 mbl and 613.5-631.4 mbl in borehole KFM02A. They occur as blocky patches along the azimuths of 0 –90°N and 180-360°N in the BHTV amplitude log (Figure 19). The latter interval obscured some features that seem to be a borehole breakout zone.

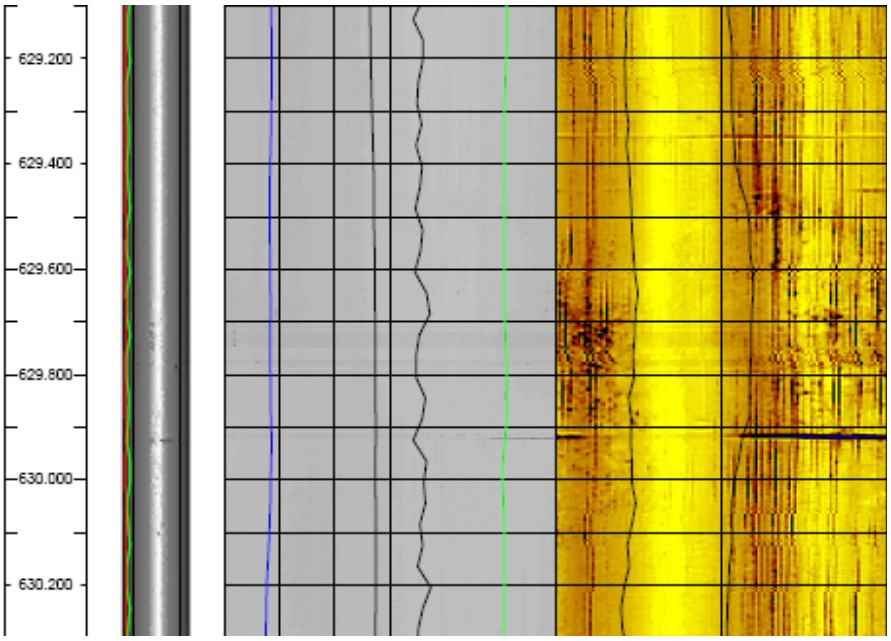

Figure 19: A section (629.1- 630.3 mbl) with a sticky zone in borehole KFM02A. The sticky zone is presented by the blocky patches in BHTV amplitude log.

5.2 Borehole Breakouts

5.2.1 KFM01B

24 borehole breakouts with a sum length of about 203 m were identified between 47 and 499 mbl in borehole KFM01B. In other words, borehole breakouts existed at almost 41% of the entire borehole length in borehole KFM01B (Figure 20 and Table 9). Their individual lengths range from 0.8 to 43.6 m whereas the average was about 8.5 m. Eleven of the identified borehole breakouts have a length range ≥ 5m. The majority (98%) of the borehole breakouts are diametrical and contributed to a sum length of ~ 199 m. The remaining (2%) are single and contributed to a sum length of about 4 m. Almost 94% of the borehole breakouts were identified from 113-270 mbl and 398-499 mbl, respectively (Figure 20). However, the downhole distribution of borehole breakouts was less between ~ 271-398 mbl. It is noteworthy to mention here that the majority of borehole breakouts that was identified in the entire borehole are shallow (mini-borehole breakouts) and have a limited failure depth (see Figure 23) with exception of a major borehole breakout identified at ~432-435.8 mbl (regarding deep borehole breakouts, see also Figure 21). Approximately 50% of the borehole breakouts have their azimuth (σ_H) ranging from 138°-142ºN (same as σ_h ranging between 48°- 52ºN) whereas 38% have theirs within the range of 154°-166ºN (σ_h –orientation ranges between 64°-76ºN). They have a length

weighted azimuth of 146º±10ºN (that is to say σ_h –orientation of 56±10ºN) thereby belonging to B-quality according to the World Stress Map (WSM) quality ranking scheme which is essentially assigned to a high quality borehole breakout [*Zoback* 1992].

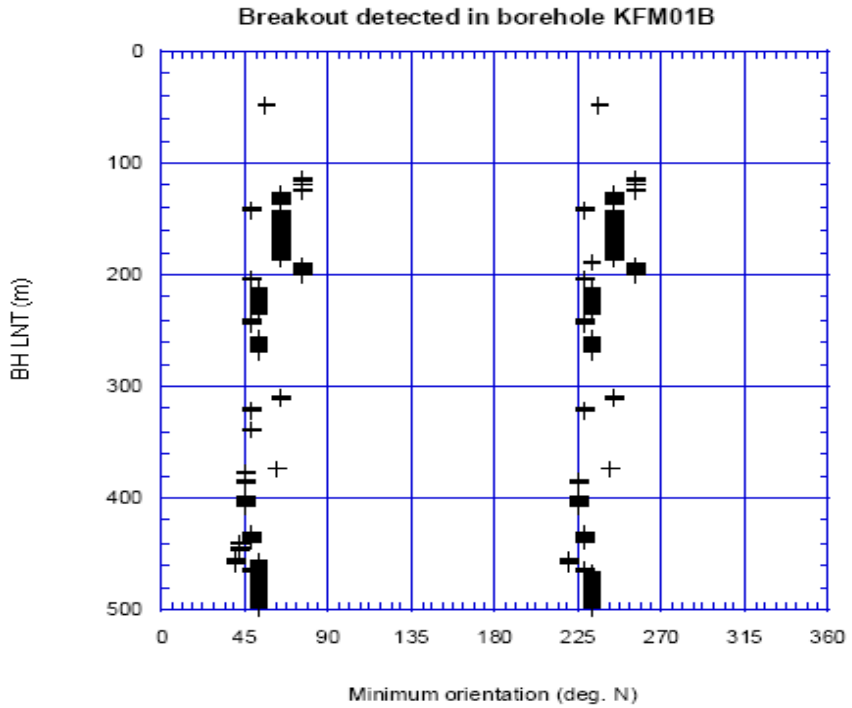

Figure 20: Downhole distribution of borehole breakouts with depth in borehole KFM01B. Note that the borehole breakouts occurred more in abundant especially from 118 to 270 mbl and from 398 to 499 mbl. Note that minimum orientation (deg.N) is referring to orientation of the minimum horizontal stress (in degrees), whereas BH LNT is referring to borehole length (in meters)

Table 9: Positively identified borehole breakouts in borehole KFM01B and estimate of σ_h-orientation.

Top depth [mbl]	Bot. Depth [mbl]	Mean depth [mbl]	BB LNT [m]	σh top [°N]	σh bot [°N]	σh mean [°N]	BB type	Deg. Clarity	Rock unit
47,2	48,4	47,9	1,2	56	56	56	Diam	Sharp	G1
112,5	117,4	114,9	4,9	76	76	76	Diam	Sharp	G2, G3
119,4	124,6	122	5,2	76	76	76	Diam	Sharp	G3
126,6	136,1	131,35	9,5	64	64	64	Diam	Medium	A, G3
139,5	142,5	141	3	48	48	48	Diam	Low	G3, P
142,6	186,2	164,4	43,6	64	64	64	Diam	Low	P, G3
186,5	188,5	187,5	2	52	52	52	Single	Sharp	G3
190,2	200,3	195,25	10,1	76	76	76	Diam	Medium	G3
202,6	203,6	203,1	1	48	48	48	Diam	Sharp	G2
210,7	235,2	222,95	24,5	52	52	52	Diam	Low-Med	G3, G2
238,8	245,2	242	6,4	48	48	48	Diam	Sharp	G3
254,6	270	262,3	15,4	52	52	52	Diam	Low-Med	G3, G2
307,9	311,1	309,5	3,2	64	64	64	Diam	Medium	G3
320,2	322,3	321,25	2,1	48	48	48	Diam	Medium	G3
338	339,2	338,6	1,2	48	48	48	Single	Low	G3
373,4	374,2	373,8	0,8	62	62	62	Diam	Sharp - Me	G3
377	377,8	377,4	0,8	45	45	45	Single	Sharp	G3
382,9	386	384,45	3,1	45	45	45	Diam	Low	G3
397,9	407,1	402,5	9,2	45	45	45	Diam	Low	G3
430,5	439	434,75	8,5	48	48	48	Diam	Sharp	G3
439	447,1	443,05	8,1	42	42	42	Diam	Sharp	G3
454,2	458,1	456,15	3,9	40	40	40	Diam	Sharp	P, G3
462,8	464,5	463,65	1,7	48	48	48	Diam	Sharp	G3
464,9	498,8	481,85	33,9	52	52	52	Diam	Sharp	G3
47,2	48,4	47,9	1,2	236	236	236	Diam	Sharp	G1
112,5	117,4	114,9	4,9	256	256	256	Diam	Sharp	G2, G3
119,4	124,6	122	5,2	256	256	256	Diam	Sharp	G3
126,6	136,1	131,35	9,5	244	244	244	Diam	Medium	A, G3
139,5	142,5	141	3	228	228	228	Diam	Low	G3, P
142,6	186,2	164,4	43,6	244	244	244	Diam	Low	P, G3
190,2	200,3	195,25	10,1	256	256	256	Diam	Medium	G3
202,6	203,6	203,1	1	228	228	228	Diam	Sharp	G2
210,7	235,2	222,95	24,5	232	232	232	Diam	Low-Med	G3, G2
238,8	245,2	242	6,4	228	228	228	Diam	Sharp	G3
254,6	270	262,3	15,4	232	232	232	Diam	Low-Med	G3, G2
307,9	311,1	309,5	3,2	244	244	244	Diam	Medium	G3
320,2	322,3	321,25	2,1	228	228	228	Diam	Medium	G3
373,4	374,2	373,8	0,8	242	242	242	Diam	Sharp - Me	G3
382,9	386	384,45	3,1	225	225	225	Diam	Low	G3
397,9	407,1	402,5	9,2	225	225	225	Diam	Low	G3
430,5	439	434,75	8,5	228	228	228	Diam	Sharp	G3
439	447,1	443,05	8,1	222	222	222	Diam	Sharp	G3
454,2	458,1	456,15	3,9	220	220	220	Diam	Sharp	P, G3
462,8	464,5	463,65	1,7	228	228	228	Diam	Sharp	G3
464,9	498,8	481,85	33,9	232	232	232	Diam	Sharp	G3

Mean orientation (σ_H = 146º±10ºN) or σ_h=56º±10ºN); sum length of borehole breakouts = 203.3m

Keys:
A = amphibolites; G1 = Granite, fine-to medium-grained; G2 = Granite, granodiorite and tonalite, metamorphic, fine-to medium-grained; G3 = Granite to granodiorite, metamorphic, medium-grained; P = Pegmatite.

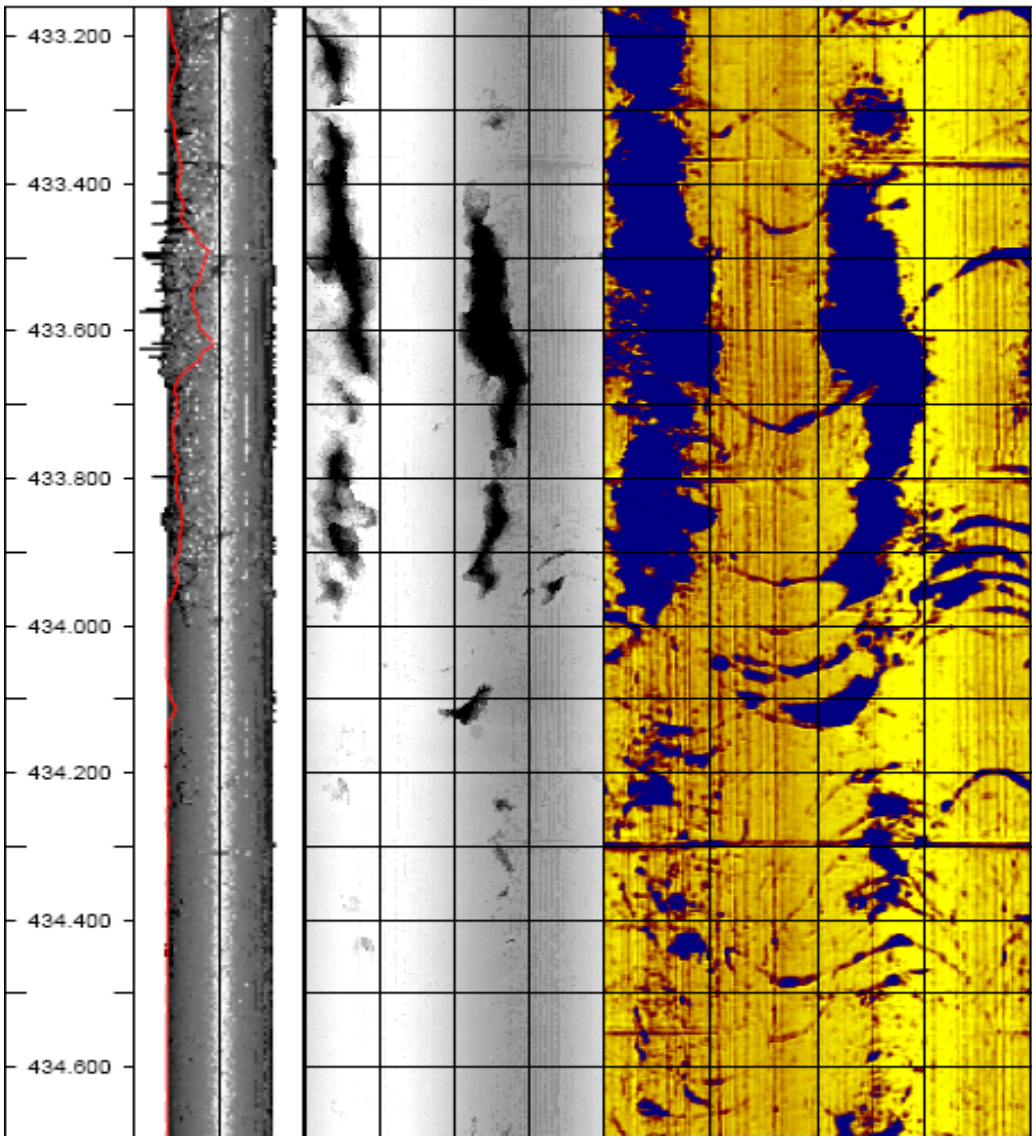

Figure 21: Diametrical borehole breakouts identified from 433.2-434.7 mbl in borehole KFM01B. This is the most outstanding deep borehole breakout observed in the borehole. The borehole breakout is visible in three of the BHTV logs (caliper 3D, traveltime and amplitude log. Note that the breakout was intersected with several diagonal fractures.

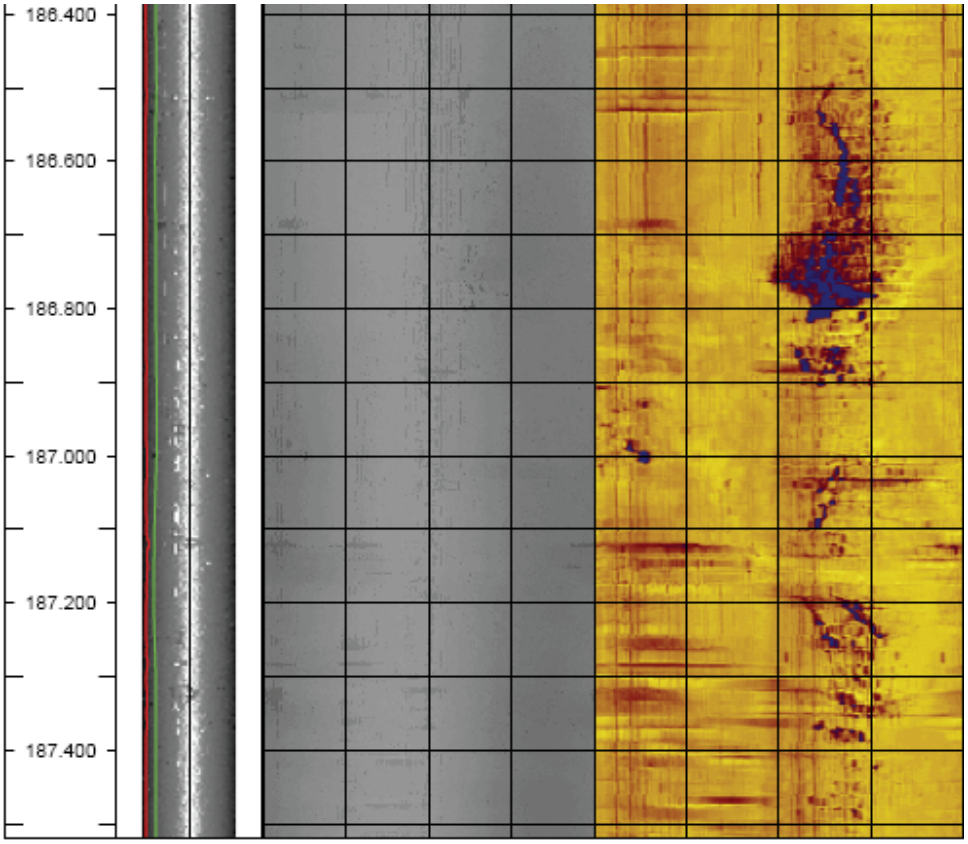

Figure 22: Single borehole breakout identified at 186.4 – 187.5 mbl in boreholeKFM01B. The borehole breakout is only visible in the BHTV amplitude log and appears only on one side of the borehole (right)

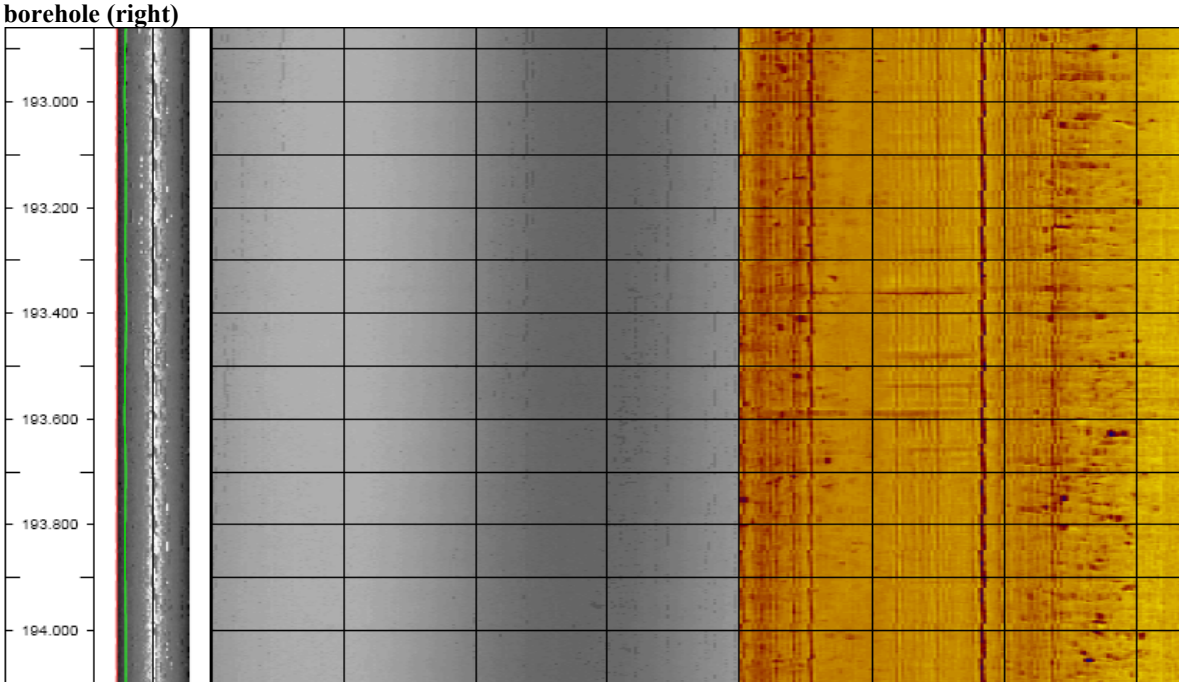

Figure 23: Example of shallow/low borehole breakout identified in borehole KFM01B from a depth range of about 192.9 to 194.1 mbl. The breakout was only visible in the BHTV amplitude log and appears on both sides of the borehole.

5.2.2 KFM02A

54 borehole breakouts with a sum length of about 266 m were identified from 99 to 1002 mbl in borehole KFM02A. This may also mean that borehole breakouts were identified at almost 30% of the entire cored part of the borehole (Figure 24 and Table 10). Their individual lengths range from 0.5 to 34.3 m and their average length was about 4.9 m. The majority of the identified borehole breakouts (65%) are diametrical (Figure 25) and contributed to a sum length of about 231 m. The remaining (35%) are single and contributed to 40 m (Figure 26). Both deep and shallow borehole breakouts were observed, but the majority (>80%) are shallow breakouts (Figure 27) whereas only few could be considered as deep borehole breakouts (< 20%). The three most prominent sections with deep borehole breakouts were encountered at 422.2-423.1 mbl; 497.2 – 498.2 mbl; and 483.1 – 483.6 mbl, respectively (Figure 25). Also, borehole breakouts were combined with washouts from a depth range of ~296 to 296.5 mbl (Figure 28). Likewise, some of the borehole breakouts were concealed by spiral grooves, a typical example is shown in Figure 29, where borehole breakout was partially concealed by spiral grooves at a depth interval ~ 985.1 to 1001.8 mbl. Borehole breakouts were identified more in abundance within the interval 500 to 1002 mbl. This may also suggest that borehole breakouts are sparsely distributed at the shallow surface (i.e., between the depth range 99-500 mbl). More so, many shifts in orientation of borehole breakouts were noted in the shallow part of the borehole, particularly from 99 to 499 mbl. The majority (89%) of borehole breakouts have azimuths ranging between 135º-159ºN (σ_H). They have a length weighted mean of 146º±18ºN (σ_H), which is also the same as σ_h-orientation of 56º±18ºN. This also results to B-quality borehole breakouts according to the World Stress Map ranking scheme, which is essentially assigned to high quality borehole breakouts *Zoback* [1992].

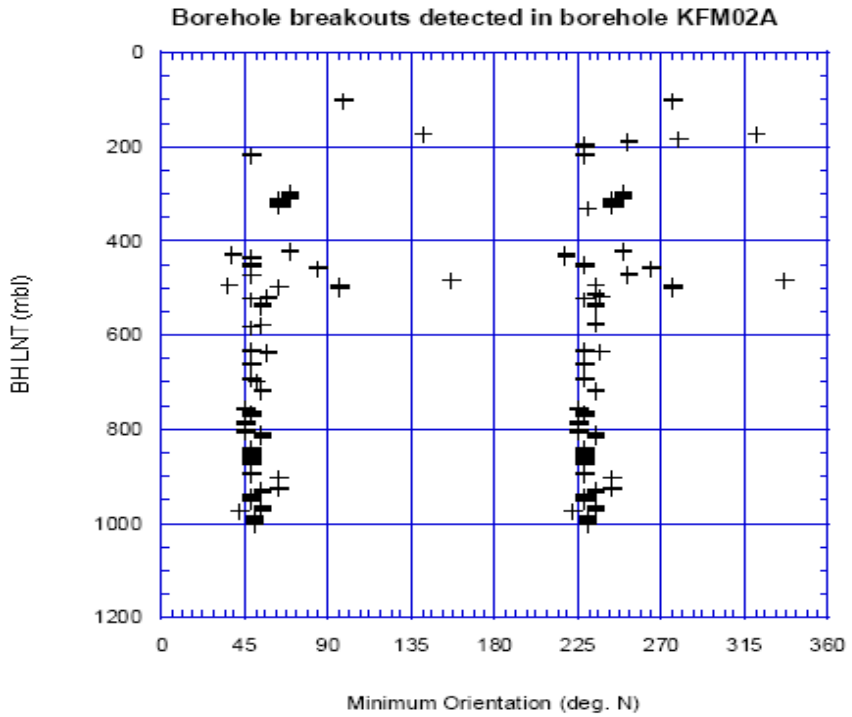

Figure 24: Downhole distribution of borehole breakouts versus depth in borehole KFM02A.

Table 10: Positively identified borehole breakouts in borehole KFM02A.

Top depth [mbl]	Bot. Depth [mbl]	Mean depth [mbl]	BB LNT [m]	σh top [°N]	σh bot [°N]	σh mean [°N]	BB type	Deg. Clarity	Rock unit
98,8	103,3	101,05	4,5	96	98	96	Diam	Medium	G3
174,2	175,3	174,75	1,1	141	141	141	Diam	Medium	G3,G2
181,7	183	182,35	1,3	282	279	279	Single	Medium	G3
187,7	189,6	188,65	1,9	261	252	252	Single	Medium	G2,G3
192,9	195	193,95	2,1	231	228	228	Single	Medium	G2
196,7	198,2	197,45	1,5	42	42	42	Single	Medium	G2,G3
198,4	200,9	199,65	2,5	258	258	258	Single	Medium	G3,A
216,7	220,4	218,55	3,7	48	48	48	Diam	Medium	G3
296,1	309,8	302,95	13,7	69	69	69	Diam	Medium	G3
311,4	322,4	316,9	11	63	63	63	Diam	Medium	A,G3
323,6	326,2	324,9	2,6	63	63	63	Diam	Medium	G3
329,3	330,4	329,85	1,1	230	230	230	Single	Medium	G3,A
419,5	424,3	421,9	4,8	69	69	69	Diam	Sharp	G3
426,6	430,1	428,35	3,5	38	38	38	Diam	Medium	G3
430,1	433	431,55	2,9	218	218	218	Single	Low	G3
433,4	435,5	434,45	2,1	48	48	48	Single	Low	G3
448,4	454,3	451,35	5,9	48	48	48	Diam	Low	G3
454,5	456,1	455,3	1,6	48	48	48	Single	Low	G3
456,4	460,5	458,45	4,1	84	84	84	Diam	Medium	G3
470,7	472,2	471,45	1,5	252	252	252	Single	Medium	A,G3
473,6	474,9	474,25	1,3	48	48	48	Single	Medium	G3
482,8	483,7	483,25	0,9	156	156	156	Diam	Sharp	G3
492,5	494,1	493,3	1,6	234	234	234	Single	Medium	G3
494,1	494,6	494,35	0,5	36	36	36	Diam	Medium	G3
494,8	496,1	495,45	1,3	96	96	96	Diam	Sharp	G2
496,1	497,2	496,65	1,1	63	63	63	Single	Medium	G2
497,2	498,8	498	1,6	96	96	96	Diam	Sharp	G2
510,1	512	511,05	1,9	234	234	234	Single	Medium	G1
517,7	520,2	518,95	2,5	57	57	57	Diam	Low	G3
520,3	521,8	521,05	1,5	57	57	57	Single	Low	G3
521,9	533,4	527,65	11,5	48	48	48	Diam	Medium	G3
534	539,1	536,55	5,1	54	54	54	Diam	Medium	G3
576,8	579,8	578,3	3	54	54	54	Diam	Medium	G3
583	584,1	583,55	1,1	48	48	48	Single	Low	G2
631,4	632,1	631,75	0,7	48	48	48	Diam	Low	G2
632,2	634,3	633,25	2,1	48	48	48	Single	Low	G2,G3
634,3	637,9	636,1	3,6	57	57	57	Diam	Medium	G3
637,9	641,4	639,65	3,5	57	57	57	Single	Medium	G3
659,3	665	662,15	5,7	48	48	48	Diam	Medium	G3
690,4	694,8	692,6	4,4	48	48	48	Diam	Medium	G3
697	700	698,5	3	51	51	51	Diam	Low	G3
715,8	721,2	718,5	5,4	54	54	54	Diam	Low-Med	G3
755,3	758,8	757,05	3,5	45	45	45	Diam	Low-Med	G3
762,4	772,2	767,3	9,8	48	48	48	Diam	Low	G3
782,5	800,2	791,35	17,7	45	45	45	Diam	Sharp-Low	G3,P
802,3	806,3	804,3	4	45	45	45	Diam	Medium	G3,A
807,6	817,7	812,65	10,1	54	54	54	Diam	Medium	A,G3,P
839,8	874,1	856,95	34,3	48	48	48	Diam	Low-Med	G2
894,2	896,7	895,45	2,5	48	48	48	Diam	Low	G3
923,7	925,7	924,7	2	63	63	63	Diam	Sharp-Med	G2
925,8	935,4	930,6	9,6	54	57	54	Diam	Low-Med	G2
941,1	952,1	946,6	11	48	48	48	Diam	Low-Med	G3
964,2	972,8	968,5	8,6	54	54	54	Diam	Low	G3
985,2	1001,8	993,5	16,6	50	50	50	Diam	Low	G3
98,8	103,3	101,05	4,5	276	276	276	Diam	Medium	G3

174,2	175,3	174,75	1,1	321	321	321	Diam	Medium	G3,G2
216,7	220,4	218,55	3,7	228	228	228	Diam	Medium	G3
296,1	309,8	302,95	13,7	249	249	249	Diam	Medium	G3
311,4	322,4	316,9	11	243	243	243	Diam	Medium	A,G3
323,6	326,2	324,9	2,6	243	243	243	Diam	Medium	G3
419,5	424,3	421,9	4,8	249	249	249	Diam	Sharp	G3
426,6	430,1	428,35	3,5	218	218	218	Diam	Medium	G3
448,4	454,3	451,35	5,9	228	228	228	Diam	Low	G3
456,4	460,5	458,45	4,1	264	264	264	Diam	Medium	G3
482,8	483,7	483,25	0,9	336	336	336	Diam	Sharp	G3
494,1	494,6	494,35	0,5	216	216	216	Diam	Medium	G3
494,8	496,1	495,45	1,3	276	276	276	Diam	Sharp	G2
497,2	498,8	498	1,6	276	276	276	Diam	Sharp	G2
517,7	520,2	518,95	2,5	237	237	237	Diam	Low	G3
521,9	533,4	527,65	11,5	228	228	228	Diam	Medium	G3
534	539,1	536,55	5,1	234	234	234	Diam	Medium	G3
576,8	579,8	578,3	3	234	234	234	Diam	Medium	G3
631,4	632,1	631,75	0,7	228	228	228	Diam	Low	G2
634,3	637,9	636,1	3,6	237	237	237	Diam	Medium	G3
659,3	665	662,15	5,7	228	228	228	Diam	Medium	G3
690,4	694,8	692,6	4,4	228	228	228	Diam	Medium	G3
697	700	698,5	3	231	231	231	Diam	Low	G3
715,8	721,2	718,5	5,4	234	234	234	Diam	Low-Med	G3
755,3	758,8	757,05	3,5	225	225	225	Diam	Low-Med	G3
762,4	772,2	767,3	9,8	228	228	228	Diam	Low	G3
782,5	800,2	791,35	17,7	225	225	225	Diam	Sharp-Low	G3,P
802,3	806,3	804,3	4	225	225	225	Diam	Medium	G3,A
807,6	817,7	812,65	10,1	234	234	234	Diam	Medium	A,G3,P
839,8	874,1	856,95	34,3	228	228	228	Diam	Low-Med	G2
894,2	896,7	895,45	2,5	228	228	228	Diam	Low	G3
923,7	925,7	924,7	2	243	243	243	Diam	Sharp-Med	G2
925,8	935,4	930,6	9,6	234	234	234	Diam	Low-Med	G2
941,1	952,1	946,6	11	228	228	228	Diam	Low-Med	G3
964,2	972,8	968,5	8,6	234	234	234	Diam	Low	G3
985,2	1001,8	993,5	16,6	230	230	230	Diam	Low	G3

Mean orientation (σ_H = 156º±18ºN or σ_h = 56º±18ºN); sum length of borehole breakouts = 266.4 m

Keys:

A= Amphibolites; B (m) = bottom depth in meters; B (ºN) = bottom orientation in degree north; BB = borehole breakout; D = diametrical breakouts;

σ_{hmin} orient. = Minimum horizontal principal stress orientation; G1= Granite, fine-to medium-grained; P = Pegmatite, pegmatitic granite; G2 = Granite, granodiorite and tonalite, metamorphic, fine-to medium-grained; G3 = Granite to granodiorite, metamorphic, medium- grained

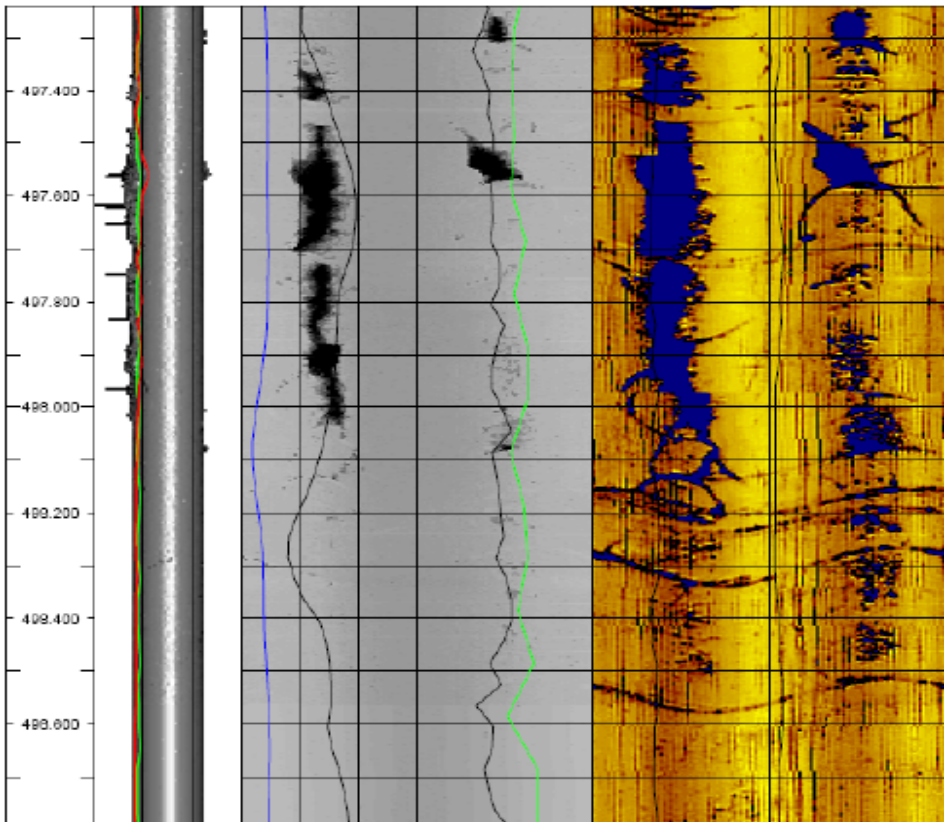

Figure 25: Diametrical and deep borehole breakout identified at 497.2-498.1 mbl in borehole KFM02A. The borehole breakout was clearly observed in three of the BHTV logs.

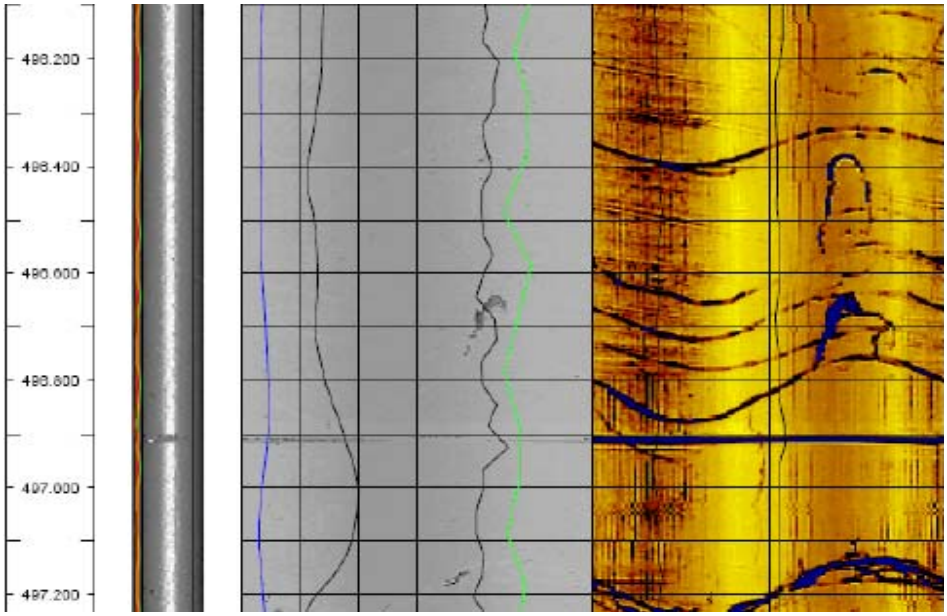

Figure 26: A single borehole breakout identified at 496.1-497.2 mbl in borehole KFM02A. The borehole breakout was intercepted with several diagonal fractures and was only visible in the BHTV amplitude log.

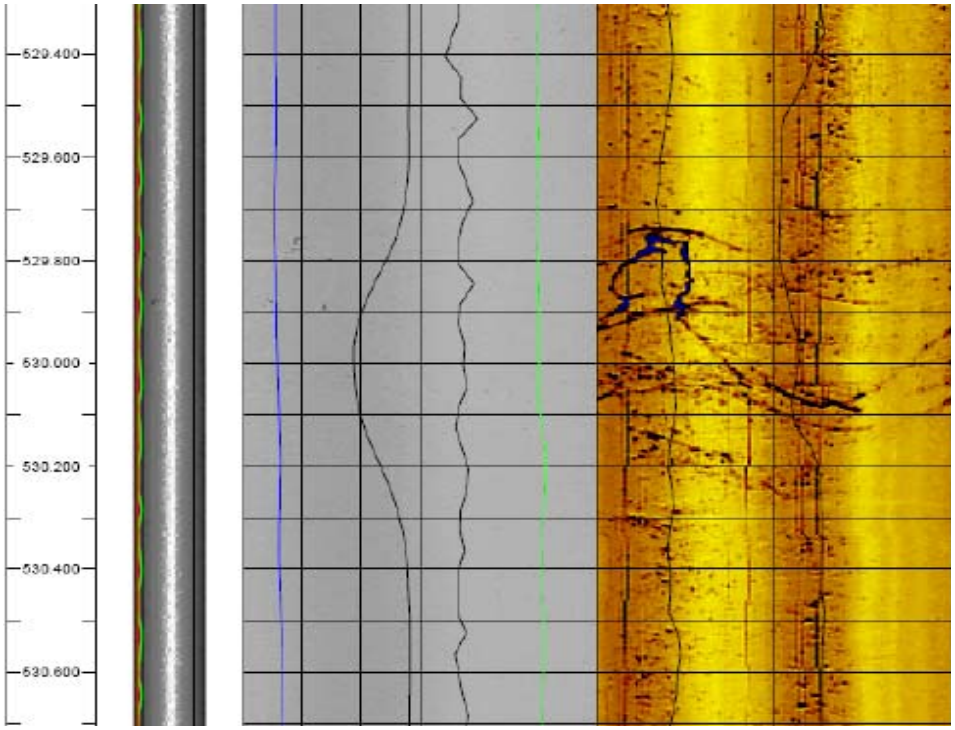

Figure 27: A shallow/low borehole breakout identified between 529.3 – 530.7 mbl in borehole KFM02A. Note that the majority of borehole breakouts observed in the borehole are Shallow breakouts.

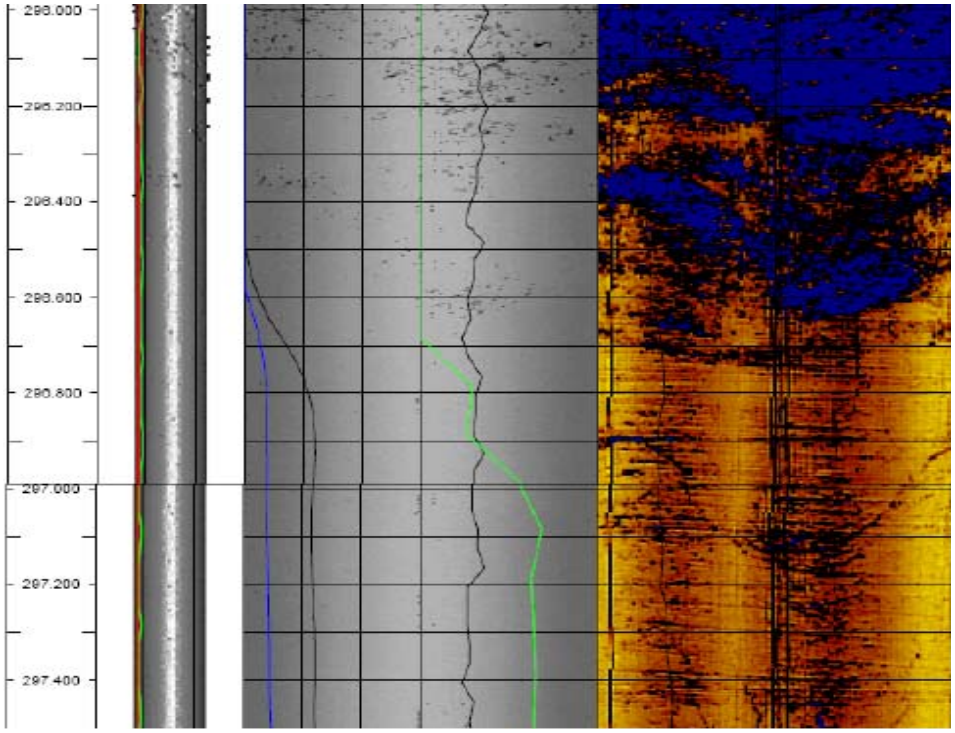

Figure 28: Borehole breakout identified at 296-297.5 mbl in borehole KFM02A. The breakout was partly concealed by a washout at 296-.296.7 m.

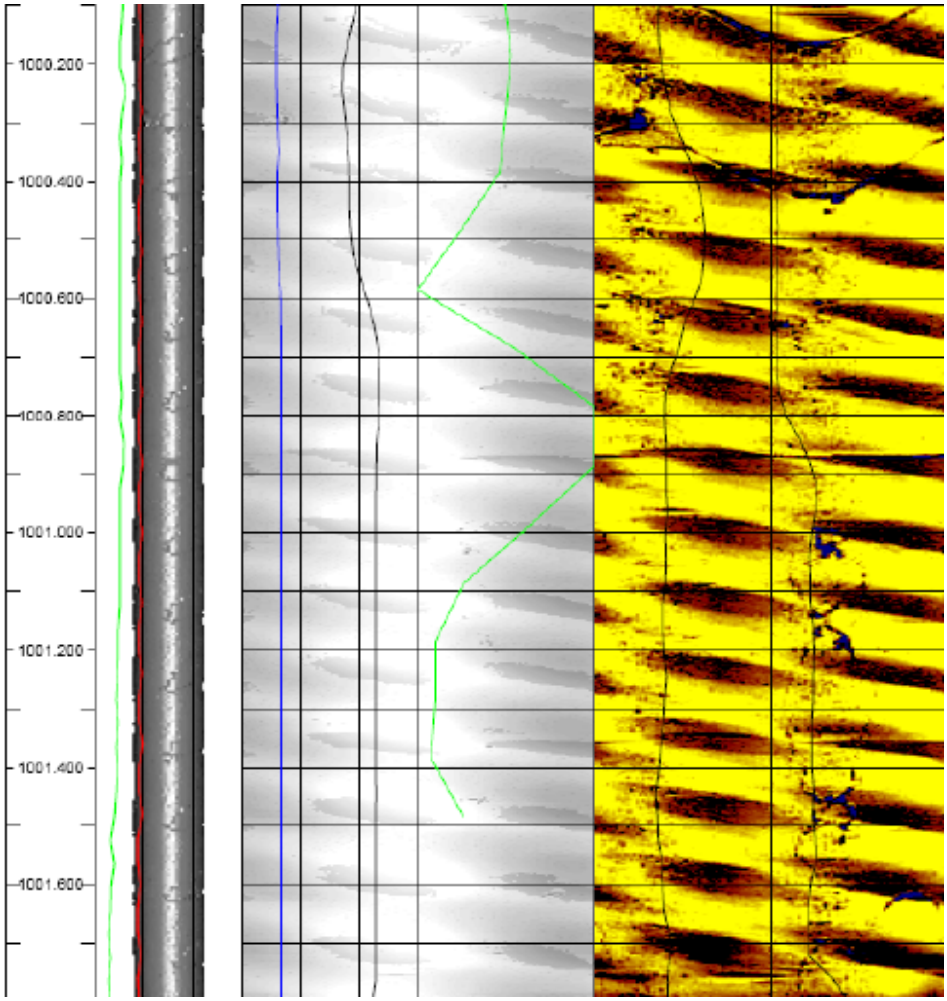

Figure 29: Borehole breakout partially concealed by spiral grooves at 1000.1- 1001.8 mbl in borehole KFM02A.

6.0 INFLUENCE OF GEOLOGY AND STRUCTURES ON ROCK STRESS ORIENTATIONS AND DOWNHOLE DISTRIBUTION OF BOREHOLE BREAKOUTS

6.1 Results

6.1.1 Borehole KFM01B

Borehole breakouts are not evenly distributed with depth in borehole KFM01B. The two most prominent sections where borehole breakouts were identified in abundance occur from 113 to 270 mbl and 398 to 499 mbl (Figure 20). However, in between this range i.e., from 271 to 398 mbl, borehole breakouts tend to be sparsely distributed. More so, slight shift in borehole breakout azimuth was observed from 113 to 190 mbl where the majority of azimuths is ranging from 154º to 166ºN, thus above the mean azimuth of 146ºN thereby result to slight scatter as observed in this section (Figure 30). Figure 30 also illustrates a correlation of borehole breakouts with lithological rock units and deformation zones. Figure 31 is a legend to Figure 30. Table 11 shows the number of borehole breakouts identified in various rock units in borehole KFM01B.

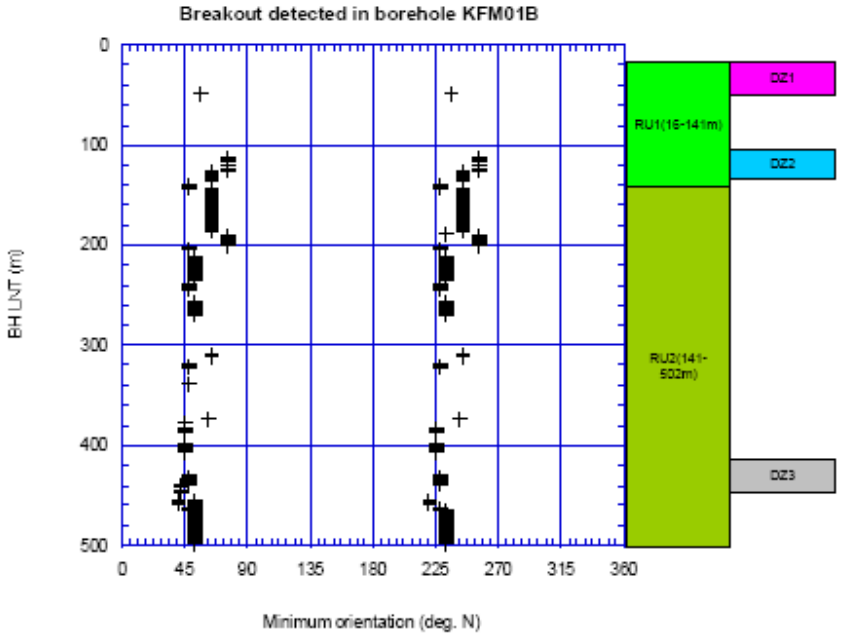

Figure 30: Correlation of borehole breakouts, to lithological rock units and deformation zones in borehole KFM01B.

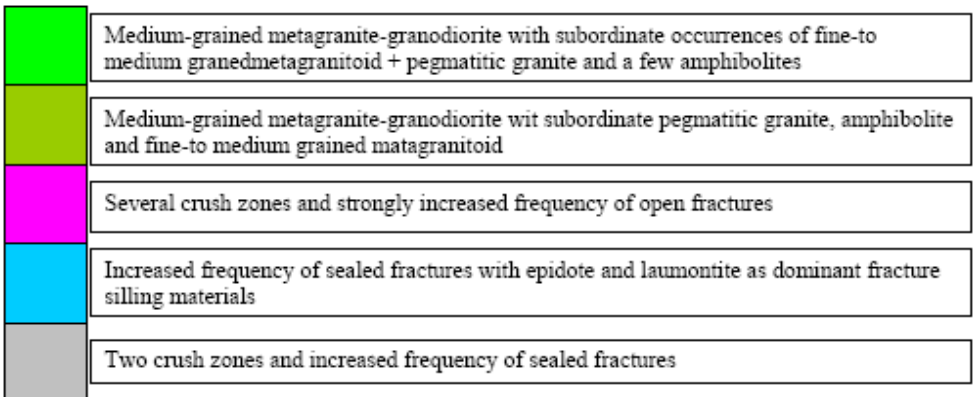

Figure 31: The keys describing lithological rock units and the deformation zones in borehole KFM01B.

Table 11: A table illustrating the number of borehole breakouts picked in various rock units in borehole KFM01B

Rock unit	Length (m)	Number of borehole breakouts observed
G2	1.3	1
G3	96.1	15
A, G3	8.8	1
G2, G3	44.3	3
G3, P	52.8	4

Keys
A = ampbibolite; G1 = granite, fine –to medium grained; G2 = granite, granodiorite, and tonalite, metamorphic, fine –to medium –grained; G3 = granite to granodiorite, metamorphic, medium –grained; P = pegmatitic granite

Table 11 indicated that the majority (> 70%) of the borehole breakouts identified in the borehole is mainly on rock unit G3. In other words, almost 15 out 24 identified borehole breakouts with a sum length of about 96.1 m were encountered in rock unit G3. Apart from this value, several other borehole breakouts were still picked where the major rock unit (G3) established a common contact point (coalesce) with other subordinate rock units. Three examples of such instances are:

1) One borehole breakout with a length of about 8.8 m has a common contact point between rock unit A and G3;
2) Three borehole breakouts with a total length of about 44.3 m have a contact point between rock unit G2 and G3; and lastly,
3) Four borehole breakouts with a total length of about 52.8 m have a contact between G3 and P.

Figure 30 shows the correlation of borehole breakouts with the lithologial rock unit and deformation zones. The result indicated that the deformation zone DZ1 (a section with a several crushed zones) was strongly correlated with the borehole breakout identified from 47.2 to 48.4 mbl. However, this deformation zone does not generate any discontinuity in the borehole breakout orientation since the average orientation in that part of the borehole

is 146°N. The major rock unit in this part of the borehole is rock unit G3. The second deformation zone DZ2 (increased frequency of sealed fractures with epidote and laumonite as dominant fracture filling minerals) was strongly correlated to the borehole breakout identified from 107 to 135 mbl but the influenced is assumed to extend until 200 mbl. Furthermore, four rock units (A, G2, G3, and P) coexisted in this part of the borehole. This may simply mean that the coexistence of several rock units and deformation zone DZ2 contributed much to the shift in borehole breakout orientation identified in borehole KFM01B at c. 200 mbl, see Figure 30. The last deformation zone, DZ3 (a section comprising two-crushed zones and increased frequency of sealed fractures) was strongly correlated to the borehole breakouts identified from 415 to 454 mbl. The maximum orientation of borehole breakouts at this part of the borehole ranges between 222° and 228°N. Thus, this could be considered as a continuous section. More so, this part of the borehole is essentially of a rock unit (G3). In summary, deformation zones DZ1 and DZ3 do not have much impact or influences on borehole breakout orientation which in both sections of the borehole is homogenous. But deformation zone DZ2 and the contact point where several rock units coexisted contributed to the shift in stress orientation identified in the borehole.

6.1.2 Borehole KFM02A

Borehole breakouts are observed over extended intervals along the borehole wall but tend to be evenly distributed especially between 500-1002 mbl. The initial 99-500 mbl is sparsely distributed. Also, this range is associated with a shift in rock stress orientations. In addition, the σ_{H}- orientation of borehole breakouts at the upper intervals are ranging between 126°N to 66°N (i.e., σ_{h} – orientation ranges between 36° to 156°N). This may suggest that the stress field is inconsistent not only regionally but also varies with depth. Borehole breakouts are observed in the entire rock unit but the majority of them were mainly identified in rock unit G3. For instance, 33 out of a total of 54 borehole breakouts, with a total length of about 156 m identified in the borehole were mainly found in rock unit G3. Also, 3 borehole breakouts with a sum length of about 4 m were found in rock unit G2. Several other borehole breakouts were still found where rock unit G3 coexisted with lesser rock units like A, G3, and P (Table 12). Table 12 depicted three of such instances. For example, at depth intervals between 174.2-175.3 mbl and 187.7-189.6 mbl, respectively, borehole breakouts were found to coalesce between rock units G3 and G2. More so, a borehole breakout was identified between the depth range 470.2-472.2 mbl to coalesce between rock units G3 and A.

Figure 32 also illustrate correlation of borehole breakouts with lithological rock units and deformation zones. Figure 33, is a legend to Figure 32. Table 12 shows sections in borehole KFM02A with scatter in orientation of borehole breakouts, the various rock units involved, the deformation zones and the number of borehole breakouts identified in each borehole interval.

In Figure 32, it was observed that three out of a total of ten deformation zones identified in the borehole were strongly correlated to the section of the borehole with rock stress discontinuities. For example, the deformation zone DZ3 (increased frequency of both sealed and open fractures) was suspected to influence the orientation of borehole

breakouts identified between 174-190 mbl. The deformation zone DZ5 (increased frequency of sealed fractures, but to some extent open fractures) was suspected to contribute to the re-orientation of borehole breakouts observed between 296-310 mbl. Lastly, the deformation zone DZ6 (wide zone with increased frequency of both open and sealed fractures) was the major deformation zone in the borehole and was suspected to have contributed to the re-orientation of borehole breakouts observed from 419 to 499 mbl. It appears that deformation zones DZ1, DZ2, DZ4, DZ7, DZ8, DZ9 and DZ10 do not have much influence in orientation of borehole breakouts in the borehole (Figure 32 and Figure 33).

Conclusively, deformation zones DZ3, DZ5, DZ6 and the rock unit G2, G3 and to a greater extent at the points were various rock units coexisted were suspected to contributed to discontinuities in breakouts orientations in borehole KFM02A.

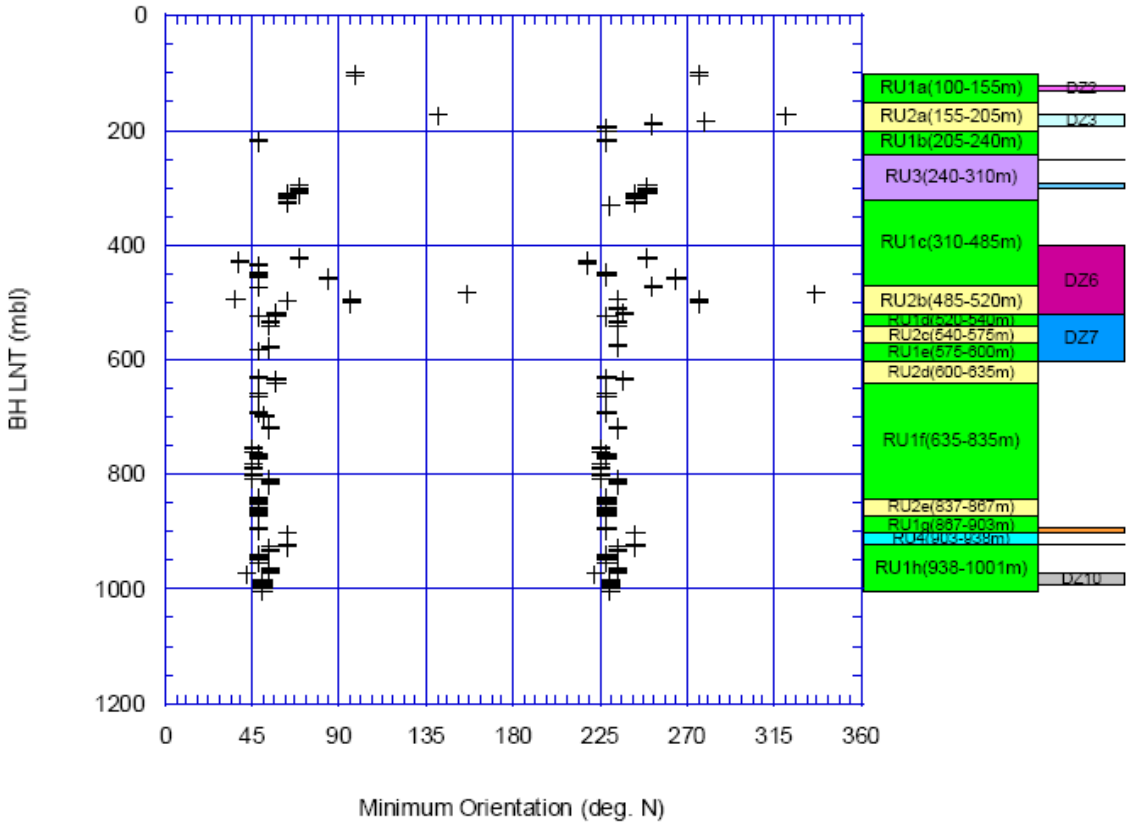

Figure 32: Correlation of borehole breakouts to lithological rock units and deformation zones in borehole KFM02A.

Keys

Keys

	Medium-grained metagranite to granodiorite with subordinate occurrences of amphibolite and pegmatitic granite
	Heterogenous interval, predominantly with a fine- grained metagranitoid
	Vuggy metagranite with minor occurrences of fine-grained metagranitoid, amphibolite and pegmatitic granite
	Homogeneous interval of a tonalitic variety of the fine-grained metagranitoid with minor occurrences of amphibolite and pegmatitic granite

DZ2	Increased frequency of open fractures with several crsuh zones
DZ3	Increased frequency of both sealed and open fractures
DZ4	Crush zone
DZ5	Increased frequency of sealed, but to some extent also open fractures
DZ6	Wide zone with increased frequency of both open and sealed fractures
DZ7	Increased frequency of sealed fractures, but relatively few open fractures
DZ8	Increased frequency of open fractures
DZ9	Increased frequency of sealed fractures
DZ10	Slightly increased frequency of both open and sealed fractures

Figure 33: The keys showing the lithological rock units and the deformation zones in borehole KFM02A.

Table 12. Sections in borehole KFM02A with scatter in orientation of borehole breakouts, the various rock units involved and the deformation zones.

BH section (mbl)	σ_H-orientation	Breakout length (m)	Deformation zone	Rock units
174.2 – 175.3	129	1.1	DZ3	G3, G2
181.7 – 183	9	1.3	DZ3	G3
187.7 – 189.6	162	1.9	DZ3	G3, G2
296.1 - 309.8	159	13.8	DZ5	G3
419.5 – 424.3	159	4.8	DZ6	G3
456.4 – 460.5	174	4.1	DZ6	G3
470.7 – 472.2	162	1.5	DZ6	A, G3
482.8 – 483.7	66	0.9	DZ6	G3
494.8 – 496.1	6	1.3	DZ6	G2
496.1 – 497.2	153	1.1	DZ6	G2
497.2 – 498.8	6	1.6	DZ6	G2

A = ampbibolite; G1 = granite, fine –to medium grained; G2 = granite, granodiorite, and tonalite, metamorphic, fine –to medium –grained; G3 = granite to granodiorite, metamorphic, medium – grained; P = pegmatitic granite; BH = Borehole; mbl = meter borehole length; m = meter.

7.0 CORRELATION OF MWD PARAMETERS WITH BOREHOLE BREAKOUTS.

Borehole breakouts were only correlated with MWD parameters in borehole KFM02A. The correlated parameters are: (i) water flow, (ii) water pressure, (iii) rotation speed, (iv) rotation pressure and (v) penetration rate.

7.1 Correlation of MWD parameters within a borehole section with borehole breakouts

Interval 419-425 mbl is a section in borehole KFM02A with a deep borehole breakout (Figure 34). This interval belongs to rock unit G3 (granite to granodiorite, metamorphic, medium –grained) and occurs across a deformation zone DZ6 (wide zone with increased frequency of both open and sealed fractures).

The plot of water flow has an average value of 40 lit/min (419-424 mbl) but was declined to 35 lit/min in the remaining interval (424-425 mbl).

Water pressure is not consistent throughout the investigated intervals but a mean value of ~30 bars could be inferred.

Rotation speed was constant (1000 rpm) throughout the entire intervals investigated (419-425 m).

The rotation pressure varies in the entire interval, for instance, the rotation pressure was about 220 bars at the inception (419 m) but declined to towards the depth (425 m) to about 120 bars.

Penetration rate on the other hand varies in the entire section, for example, at the inception (419 m), penetration rate was increased from 10 to 18 cm/min but declined to about 15 cm/min towards the depth. However, from 419-423 mbl, an average value of about 10 cm/min could be inferred.

Nevertheless, in this study, the correlation of MWD parameters is based on the correlated points (points with similar trends linked together with interpolation lines).

Eight points with similar trend were correlated, and the entire amount of points indicated sharp decline in water flow and water pressure, with increase in rotation pressure and penetration rate, while rotation speed is held constant (1000 rpm). In a simple term, the overall trend observed in the eight correlated points (Figure 34) indicated that water flow and water pressure declined from ~40 to 5 lit/min and ~30 to 2 bars, respectively, whereas the rotation pressure and penetration rate increases from 120 to 220 bars and 10 to 15 cm/min, respectively.

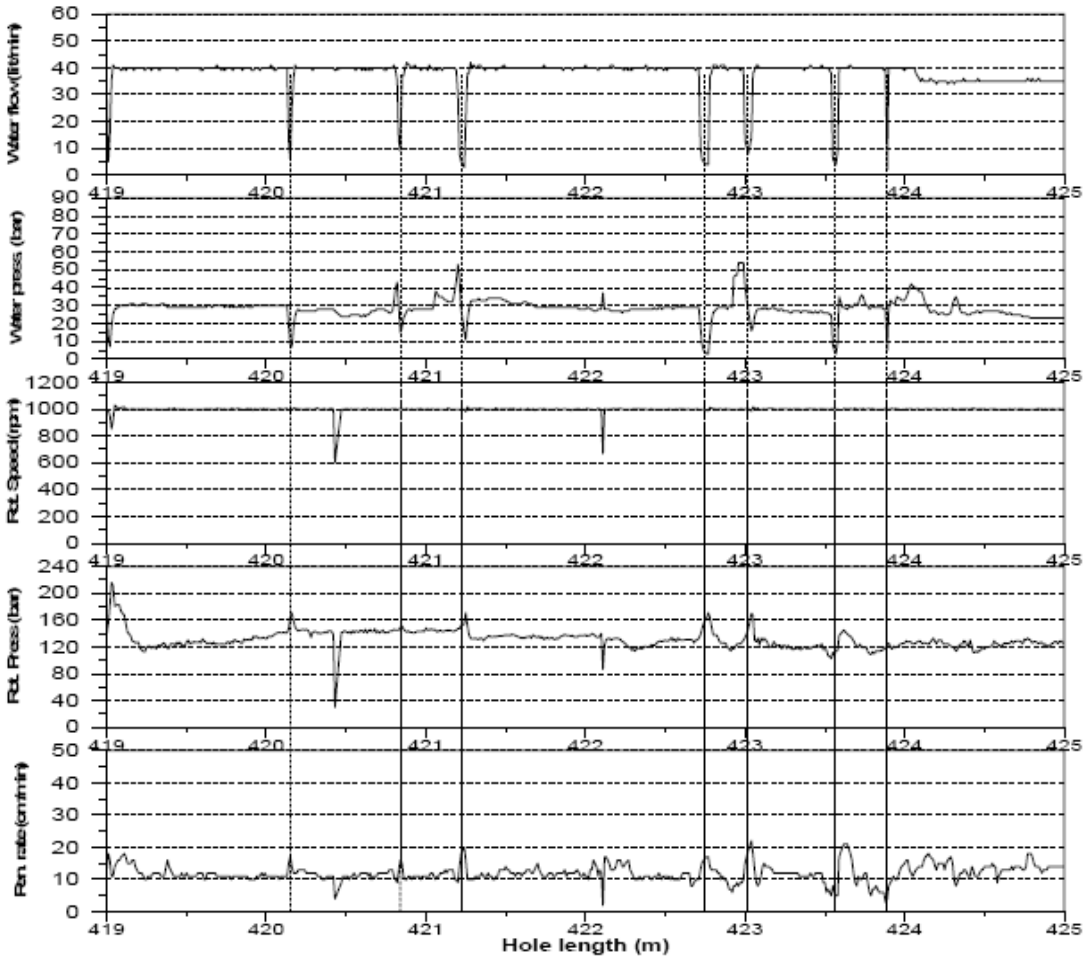

Figure 34: Correlated plot for the MWD parameters for section (419 to 425 mbl) in KFM02A with borehole breakout. Note that this section is mainly a rock unit (G3) and occurs across the major deformation zone DZ6.

7.2 Correlation of MWD parameters within a borehole section without borehole breakout

Interval 735-741 mbl is a section in borehole KFM02A without borehole breakouts (Figure 35). This interval belongs to a rock unit G3 but without deformation zones but not totally void of fractures.

The general trend in the plot suggested that the water flow rate was about 40 lit/min from ~735-736 mbl but was declined to 35 lit/min from 736.4 to 741 mbl.

Water pressure on the other hand was observed to be averagely 35 bars from 735 to 736.4 mbl but was declined slightly below 30 bars in the rest of the sections (i.e., between 736.4-741 mbl).

Furthermore, the rotation speed was constant throughout the entire interval (1000 rpm).

Rotation pressure varies throughout the entire interval studied. The rotation speed seems to be increasing from 738.2-741 mbl whereas below this interval (735-738.2 mbl), the trend was not consistent (i.e., varies over a small depth interval).

Penetration rate exhibits an increasing trend in most of the interval studied. For example, the penetration rate was about 12 cm/min) in the initial stage (735 m) but was increased to about 16 cm/min towards the end of the interval.

The general trend observed in the initial correlated point (~735.2 m) suggested that water flow, water pressure and penetration rate are directly related but are inversely related to rotation pressure and penetration rate (vice versa). While, the later correlated trend (~737.7 m) indicated that all the MWD parameters are directly related. In the later, it was indicated that (Figure 35) that water flow declined from 40 to 5 lit/min, while water pressure and rotation speed both declined from ~29 to 20 bars and 1000 to 380 rpm, respectively. Also, the rotation pressure and penetration rate, each declined from 160 to 20 bars, and 15 to 5 cm/min, respectively. Furthermore, at ~735.2 m, water flow, water pressure and rotation speed, each declined from 40 to 12 lit/min, 35 to 25 bars, and 1000 to 860 rpm, respectively. Also, at the same point the rotation pressure and penetration rate increases from 190 to 220 bars and 12 to 16 cm/min, respectively.

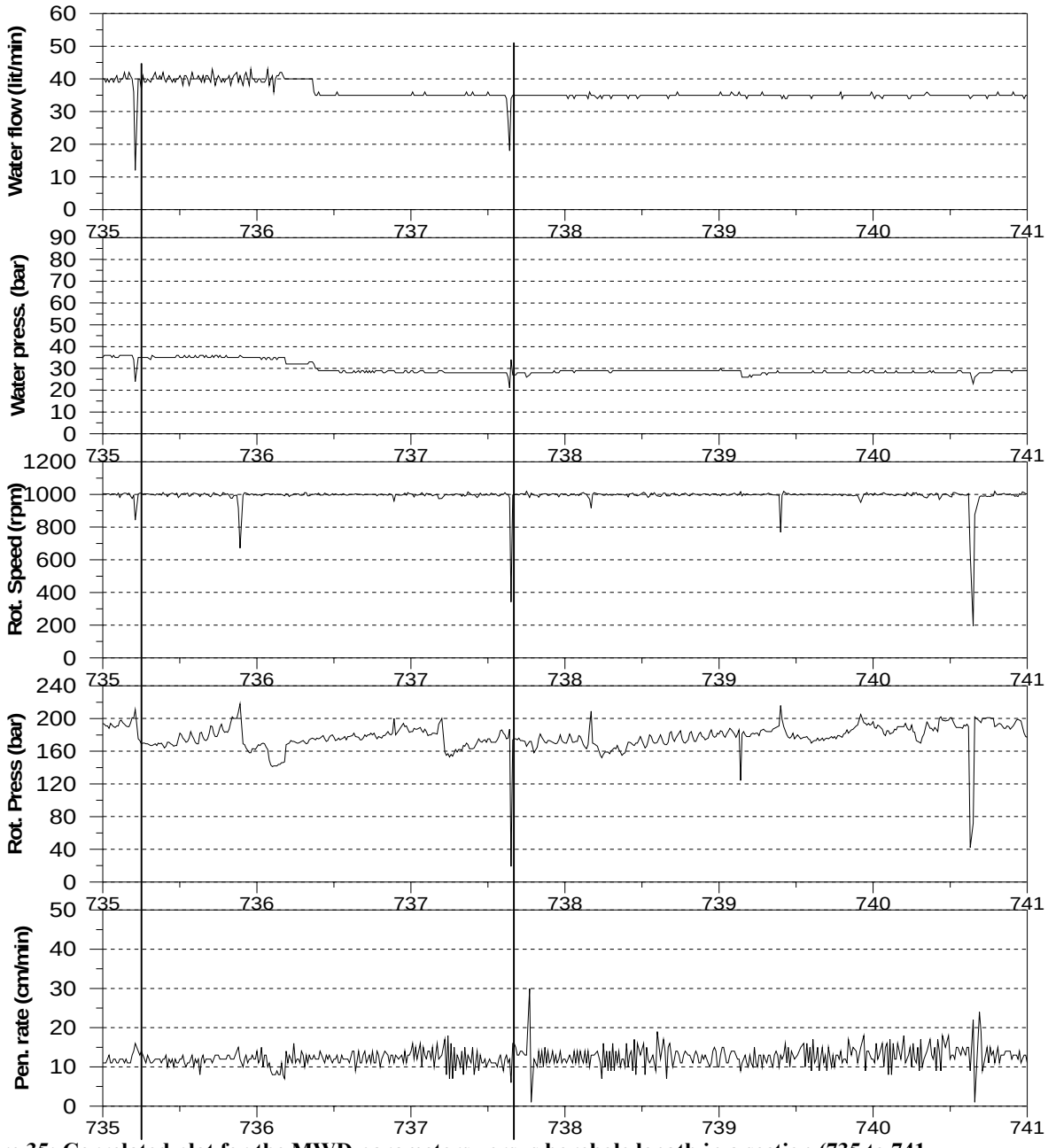

Figure 35: Correlated plot for the MWD parameters versus borehole length in a section (735 to 741 mbl) without borehole breakouts or major deformation zones.

7.3 Comparison of MWD parameters in the section with and without borehole breakouts

Because both sections with and without borehole breakouts were studied, it became imperative to compare the MWD signatories to note the differences between the sections.

In sections with borehole breakouts, it is observed that the water flow is directly related to water pressure and inversely related to both rotation pressure and penetration rate,

while rotation speed is held constant. But in the sections without borehole breakouts, the general trend in MWD parametric signatory indicated that water flow, water pressure and rotation speed are directly related. More so, the second correlated point (~737.7 m) indicated that all the MWD data parameters are directly related. In other words, the section indicated a decline in all MWD parametric signatories.

By comparing the rate of decline (water flow and water pressure) in sections with and without borehole breakouts, the result indicated that the rate is higher in the section with borehole breakouts than in the section without. For instance, in the section with borehole breakouts, water flow rate and water pressure dropped from 40 to 5 lit/min and 30 to 2 bars, respectively, whereas in the section without borehole breakouts, the water flow and water pressure dropped from 40 to 12 lit/min and 35 to 20 bars, respectively, This is the same to say that the rate of decline in water flow in the section with and without borehole breakout stands at ~88% and ~70% whereas that of water pressure stands at ~ 93% and ~43%, respectively.

Also, the section without borehole breakouts indicated that rotation speed dropped from 1000 to 380 rpm but was constant (1000 rpm) in the section with borehole breakouts.

Lastly, all the correlated points in the section with borehole breakouts indicated increase in rotation pressure and penetration rate but this was not the case for all correlated points in the interval without borehole breakouts. Both intervals contradict each other to some extent, for instance, 735.2 m indicated that rotation pressure increases from 190 to 220 bars while 737.7 m indicated that it was dropped from 160 to 20 bars. Also 735.2 m indicated that penetration rate was increased from 12 to 15 cm/min but 737.7 m indicated that it dropped from 15 to 5 cm/min.

8.0 DISCUSSION

I have organised the discussion section so that the different subchapters correspond to the primary objectives of this study, namely to: (1) determine the downhole orientation of horizontal rock stress; (2) identify zones of rock continuum; (3) study the influence of geology and structures on rock stress orientation; and (4) correlate borehole breakouts with measurement while drilling (MWD) parameters.

8.1 Orientation of horizontal rock stress

The downhole orientation of maximum horizontal stresses for the both boreholes studied is shown in Figure 20 and Figure 24. Borehole breakouts are observed over extended intervals along the borehole but with a gradual shift in stress orientation especially at the upper sections of the borehole (see Section 8.2).

In borehole KFM01B, borehole breakouts were observed in abundance between 113-270 mbl and 398-459 mbl. But in between this range (i.e., 270-398 mbl), the downhole distribution was decreased. Also, above 113 m, only one borehole breakout was observed. The general trend in σ_H – orientation of borehole breakouts suggests orientations between 130º-166ºN. However, the majority (50%) of borehole breakout sections propose σ_H-orientations between 138º to 142ºN, whereas 38% have theirs within the range of 154º -166ºN. The length weighted average orientation of σ_H is 146º±10ºN in borehole KFM01B. A total number of 24 borehole breakouts with a combined length of 203 m were observed. The quality of stress data is B-quality according to the WSM ranking scheme [*Zoback*, 1992].

In borehole KFM02A, borehole breakouts were identified more in abundance especially from 500 to 1002 mbl but with a gradual shift in stress orientation from 99 to 499 mbl. The result further indicated that the σ_H-orientation of borehole breakouts is within the range of 126º-66ºN (i.e., σ_h –orientation ranging from 36º-156ºN), with dominating (89%) orientation between 135º-159ºN (i.e., σ_h-orientation ranging between 45º-69ºN). The length weighted average orientation of σ_H is 146º±18ºN in borehole KFM02A, together with a 54 number of borehole breakouts with a total length of 266 m, thus resulting in B-quality according to the WSM ranking scheme [*Zoback*, 1992]. This orientation is consistent with σ_H-orientation reported at the Forsmark site particularly with hydraulic fracturing techniques, regional stress and plate motions. For example, the hydraulic fracturing method suggested that the σ_H-orientation at the site varies from 100° to 145°N, where as regional stress data and plate motion suggested 140° and 142°N, respectively [see, *Sjöberg et al*. 2005]

Borehole breakouts are much shorter in borehole KFM02A than in borehole KFM01B. However, because many drilling artefacts (spiral grooves) were encountered in most part of borehole KFM02A. It is possible that the total length of borehole breakouts would have been longer if no drilling artefacts were present. Hence, the current analyze may underestimate the true number of borehole breakouts in borehole KFM02A. Please refer to *Ask* [2007] for alternative explanation.

8.2 Zones of rock continuum

The results obtained from the borehole breakout study (Figure 20 and Figure 24) have demonstrated that the orientations of borehole breakouts in both boreholes studied are similar (homogeneous). In both boreholes, a slight shift (zone of discontinuity) in rock stress orientation was observed mainly at the shallow part of the boreholes, whereas the deeper part tends to be more homogeneous.

In borehole KFM01B, Figure 20 suggested that the zones of rock discontinuity existed between 113-200 mbl. At this section of the borehole, the majority (~94%) of the σ_H-orientations of borehole breakout ranges in the interval 154°-166°N, thus resulting in the length weighted average σ_H-orientation of 155°±7°N. In the same vein, the zones of rock continuity existed between 200-500 mbl, with the dominating (70%) σ_H-orientation of borehole breakouts ranging between 138°-142°N.

In borehole KFM02A, Figure 24 suggested that the zones of rock discontinuity existed within the interval 99-500 mbl. Also, at this section of the borehole, the majority (~70%) of σ_H-orientations of borehole breakout ranges within the interval 126°-66°N (which is the same as σ_h-orientation of 36°-156°N), with a length weighted average σ_H-orientation of 160°±26°N. The zones of rock continuity existed between 500-1002 mbl, with the dominating (93%) σ_H-orientation of borehole breakouts ranging between 135°-144°N in the section.

From the above, it is obvious that the orientations of borehole breakouts are more to NNW in the zones with rock discontinuity than in the zones without. The result further indicated that the rate of rock stress discontinuity is slightly higher in borehole KFM02A than in borehole KFM02A, with a span of about 24°N and 12°N, respectively (i.e., difference of 12°N).

8.3 Influence of geology and structures on rock stress orientation

The result obtained by correlating borehole breakouts with lithology and deformation zones presented in Section 6.1.1 and 6.1.2 suggested that the sections in the boreholes with rock discontinuities were well correlated to the deformation zones. Three deformation zones were identified in borehole KFM01B (Figure 30 and Figure 31) while ten deformation zones were identified in borehole KFM02A (Figure 32 and Figure 33). However, out of the three deformation zones identified in borehole KFM01B, only one, DZ2 (increased frequency of sealed fractures with epidote and laumonite as dominant filling mineral) was suspected to have contributed to the scatter in the orientation of borehole breakouts identified in the interval 113-190 mbl (Figure 30). At this section of the borehole, the σ_H-orientation of borehole breakouts ranges from 154°-166°N, thus above the mean orientation of borehole breakouts (146°N) in the entire borehole.

Likewise, in borehole kFM02A, three out ten deformation zones were suspected to have contributed to the scatter in orientation of borehole breakouts in the borehole. These deformation zones include:

1) DZ3 (increased frequency of both sealed and open fractures): This deformation zone was believed to have contributed to the scatter in orientation of borehole breakouts observed from 174-190 mbl in the borehole. At this section of the borehole, the orientation of maximum horizontal stress of borehole breakouts ranges in the interval 129°- 169°N;
2) DZ5 (increased frequency of sealed fractures, but to some extent open fractures) was suspected to have contributed to the scatter in orientation of borehole breakouts observed between 296-310 mbl. At this section of the borehole, the maximum orientation of borehole breakouts is 156°N; lastly,
3) DZ6 (wide zone with increased frequency of open and sealed fractures), is the major deformation zone that was suspected to have contributed to the scatter in orientation of borehole breakouts observed between 419-500mbl. At this section of the borehole, the maximum orientation of borehole breakouts ranges between 159°-174°N.

These deformation zones have a lot of influence on rock stress orientations. For example, *Zoback et al.* [2003] explained that the orientation of principal stresses might vary due to topography, especially in the shallow subsurface. More so, that in a borehole with widely distributed faults, fractures and planar discontinuities of many different scales and orientations, stress magnitudes at depth are limited by the frictional strength of these planar discontinuities. This assertion by *Zoback et al.* [2003] may be the plausible explanation while the majority of scatter in borehole breakouts orientation observed in both boreholes are mainly occurring towards the shallow depth of the borehole, which may as well indicate that stress fields are not continuous between shallow and large depths.

Lithology may be another explanation for the variations in rock stress orientation. It is observed that both boreholes are associated with four rock units where granite to granodiorite, metamorphic medium-grained, was indicated as the major rock unit where the majority of the borehole breakouts were detected. Also, the second most pronounced occurrence of borehole breakouts in both boreholes are in sections where different rock units are in contact. The plausible explanation of breakout formation in such a zone is that the strength of rock in those contacts varies. For example, granitic rock is a hard rock, whereas amphibolites are weaker veins; one should expect fractures to be initiated in such a contact point. The same applies to the contact with pegmatite.

In conclusion, geology and structures are suspected to have contributed immensely to the variations in rock stress orientations as observed in both boreholes.

8.4 Borehole breakouts and its correlation to MWD parameters

The results for the correlation of borehole breakouts with MWD parameters showed that borehole breakouts are well correlated with MWD data. The basis for this correlation is that MWD parameters are very sensitive to any slightest form of discontinuities in the rock, thereby reflecting such in a form of signature variations as observed in both Figure 34 and Figure 35. This may also mean that MWD parameters depict the mechanical

properties of the host rock as a result of strength variation. However, MWD data may not be able to differentiate breakouts from ordinary fractures.

Within the eight correlated points in the section with borehole breakouts (Figure 34), it was observed that the water flow is directly related to water pressure and inversely related to both rotation pressure and penetration rate, while rotation speed is held constant. This is probably because of the fact that the correlated borehole interval occurred across the deformation zone DZ6. It is expected that in such a zone that the strength of the rock should be decreased. This is absolutely in order with MWD parameters, decreasing trend in water flow and water pressure, with increasing trend in both rotation pressure and penetration rate is an indication of deep fractures at those points, which serves as conduits by which water or drilling fluid injected into the borehole to cool down the drill-bit and at the same time flush the drill cuttings to the surface are lost. This studied interval could as well impact less resistance to the drill. This is strongly in agreement with the previous report by *Ask and Ask,* [2007]. The authors reported that the higher feed force and lower drill rate at the Forsmark site resulted in a higher feed force and lower drill-bit contact, thus resulting to increases in the rock temperature, heat expansion and induced thermal stress of the rock. However, the author regretted lack of full understanding of the impacts associated with transient, 3D thermo-mechanical.

The rotation speed is constant within the borehole breakout interval, whereas it varies in the section without borehole breakouts. Because the system for MWD data collection is automatic, it is difficult to draw safe conclusions about the affect of MWD parameters [*Lennart Ekman, Pers. Comm.*, 2008].

Comparing both intervals with and without borehole breakouts, it is possible to infer that the drill parameters behaved differently when drilling in more competent rock (Figure 35). It is also possible to infer that the sections with borehole breakouts are associated with a higher frequency of fractures or fault zones than the sections without. For instance, the trend observed at ~737.7 m (Figure 35) indicated that all the drill parameters are directly related (indicating a decreasing trend in all the drill parameters). This is also in order, because it is logical that rotation speed; rotation pressure and penetration rate should decline simultaneously. For instance, it is expected that decrease energy supply should have this effect. Decline in rotation speed, rotation pressure and penetration rate could however also be indications of encountering a more competent rock with increase compressive stress thus impact more resistance to the drill.

9.0 CONCLUSIONS

This thesis presents data from boreholes KFM01B and KFM02A that are part of the Forsmark investigation site of the Swedish Nuclear Fuel and Waste Management Co (SKB). Two types of image tools, borehole televiewer (BHTV) and borehole image processing system (BIPS) have been used to reveal the stress orientation using borehole breakout methods. The objective of this report have been to: (1) determine the downhole orientation of horizontal rock stresses; (2) identify the zones of rock continuum; (3) study the influence of geology on rock stress orientation; and (4) correlate borehole breakouts with measurement while drilling (MWD) parameters.

The result from this study shows that borehole breakouts are common in both boreholes. In borehole KFM01B, borehole breakouts have been identified starting from 47 and continuing to 498 mbl. Borehole breakouts occupy 203.3 m of total 500 mbl, which corresponds to almost 41% of the entire logged borehole. Almost 85% of the identified borehole breakouts were identified from section 113-270 mbl and 398-498 mbl, respectively. The majority of the identified borehole breakouts are shallow and have a limited failure depth. In addition, almost 50% of the identified borehole breakouts have their σ_H-orientation ranging between section 138°-142°N, whereas 38% have theirs ranging between 154°-166°N. The length weighted average σ_H-orientation is 146°±10°N, which corresponds to quality B according to the WSM ranking scheme, which is essentially assigned for high quality borehole breakouts [*Zoback*, 1992].

Likewise, in borehole KFM02A, borehole breakouts are detected between 99 - 1002 mbl, but were evenly distributed (occurred more in abundant) starting from 500 m and continuing to 1002 mbl. They occur over almost 29% of the entire cored section of the borehole (≈266 out of 1002 mbl). However, shifts in the orientation of σ_H are noted mainly between the interval 99-499 mbl. The result also reveals that the σ_H-orientation from borehole breakouts are ranging in the interval 126°-66°N (i.e., σ_h = 36°-156°N), with a dominating (i.e., 89%) σ_H-orientation ranging between 135°-159°N. The length weighted average σ_H-orientation is 146°±18°N. This also results in quality B according to the WSM ranking scheme, which is essentially assigned to high quality borehole breakouts. Hence, the two boreholes yield the same average orientation with slightly larger variation in stress orientation in borehole KFM02A than in borehole KFM01B. This orientation is consistent with the σ_H -orientation previously obtained at the Forsmark site particularly with hydraulic fracturing techniques, regional stress data and relative plate motions. For example, the hydraulic fracturing method suggested that the maximum horizontal stress at the site varies from 100° to 145°N, whereas regional stress data and relative plate motion suggested 140° and 142°N, respectively.

A zone with and without rock stress continuity was identified in both boreholes and was strongly correlated to the existing geology and structure at the site. In borehole KFM01B, a heterogeneous interval existed between 47-200 mbl, which corresponds to almost 31% of the logged borehole whereas the homogeneous (a zone of rock stress continuity) section existed from 200 to 500 mbl.

Similarly, in borehole KFM02A, the heterogeneous interval (zone of rock stress discontinuity) existed between 113-499mbl which corresponds to about 43% of the entire cored part of the borehole whereas a homogeneous interval existed between 499-1002 mbl. This may suggest that the stress field varies down the hole (discontinuous). The discontinuity in σ_H-orientation is mainly due to the deformation zones that intercepted the boreholes. For example, the discontinuity identified in borehole KFM01B is a result of deformation zone DZ2 (increased frequency of open fractures with several crushed zones). Similarly, three major sets of deformation zones were identified to influence the rock stress orientation in borehole KFM02A. These deformation zones include DZ3 (increased frequency of both sealed and open fractures); DZ5 (increased frequency of sealed fracture but to an extent open fractures); and lastly;DZ6 (a wide zone with increased frequency of both sealed and open fractures). Another plausible explanation for the scatter in orientation of borehole breakouts is the coexistence of several rock units in the boreholes and also the contact points where those rock units coexisted (coalesce). In such sections of two or several interlayered rock types, the compressive strength of the rock varies. An example is the contact between granite and amphibolite. One should expect fractures to be initiated especially at the contact point of such coexistence, since granite rock is a hard rock whereas amphibolite is a weaker vein.

MWD parameters were collected in borehole KFM02A and consequently correlated with the identified borehole breakouts in the borehole. The general trend in the correlated sections indicated that borehole breakouts could be correlated by decrease in water flow rate and water pressure, and increase in rotation pressure and penetration rate. This is probably due to the fact that MWD parameters are very sensitive to any slightest fracture in the rock mass and subsequently depicts changes in rock mechanical and physical properties of the borehole wall. More so, the interval studied penetrated was penetrated in the deformation zone DZ6. Therefore, it is not a surprise if the drill parameters should behave as it does. Decrease in water flow rate and water pressure and increase in rotation pressure and penetration rate are indications of increased frequency of fractures, thereby offering less resistance to the drill and also serve as a conduit whereby water or drilling fluid injected into the borehole to cool down the drill string and the same time flush the drill cuttings to the surface is lost.

10.0 RECOMMENDATION FOR FUTURE RESEARCH

This study has demonstrated that borehole breakouts were formed in both boreholes KFM01B and KFM02A and also that the stress field was not continuous. However, the two boreholes studied may not be sufficient to ascertain the orientation of the stress fields at the entire site; therefore the following recommendations may be necessary:

1) SKB should carry out a detailed study on stress-induced elongations in more boreholes at the site, preferably the same analyses that was carried out in this study;
2) SKB should re-log the remaining boreholes; if possible BHTV and FMS should be used instead of BIPS images. This is because this study has demonstrated that BIPS images may not possibly detect most of the breakouts that were formed, since a majority of them were shallow breakouts and BIPS images can distinctly identify only major breakout zones in which clear fractures have been formed;
3) In subsequent drilling projects, it is advisable that the borehole should be cored at a reduced speed. This may reduce the rate at which spiral grooves were formed. In addition, the borehole should be logged immediately after drilling.

11.0 REFERENCES

Ask, M.V.S. (1997), In-Situ Stress from breakouts in the Danish Sector of the North Sea, *Marine and Petroleum Geology,* 14(3) 231-23.

Ask, D. (2003), Evolution of measurement related uncertainties in the analyses of overcoring rock stress data from Åspö HRL, Sweden: a case study *Int. J. Rock Mech. Min. Sci., 40. Pg. 1173-87.*

Ask, D. (2004), New developments of the Integrated Stress Determination Method and Application in the Åspö Hard Rock Laboratory, Sweden: A PhD thesis conducted at *Research Group of Engineering Geology and Geophysics, Department of Land and Water Resources Engineering, Royal Institute of technology (KTH), Sweden*.

Ask, D, (2007), Evaluation of hydraulic and overcoring stress measurements in boreholes KFM01A, KFM01B, KFM02A, KFM04A, DBT-1, and DBT-3 at the Forsmark site. SKB P-07-234.

Ask, D., and M.V.S. Ask (2007), Forsmark site investigation: Detection of potential borehole breakouts in boreholes KFM01A and KFM01B. SKB P-07-235

Babcock, E.A. (1978), Measurements of Subsurface Fractures from Dipmeter Logs, *American Association of Petroleum Geologists, Vol. 62, pg. 1111-1126, No. 7.*

Barton, C.A., M.D. Zoback, and K.L. Burns (1998), In-situ Stress Orientation and Magnitude at the Fenton Geothermal Site, New Mexico, determined from wellbore breakouts. *Geophys. Res. Lett., -*

Bell, J.S., and D.I. Gough (1979), Northwest-Southeast Compressive Stress in Alberta: Evidence from Oil Wells. *Earth and Planetary Sciences Letters, Vol. 45, pg. 475-482*.

Bell, J.S., and D.I. Gough (1981), Intraplate Stress Orientations from Alberta Oil-wells, in R.J. O'Connel, and Fyfe, W.S., eds., Evolution of the Earth: *American Geophys. Union, Geodynamic Series, Vol.5, pg.96-104.*

Berglund, J., J. Petersson, A. Wägnerud, and P. Danielsson (2004), Boremap mapping of core drilled borehole KFM01B. *SKB P-report P-04-114.* Svensk Kärnbränslehantering AB.

Claesson, L.Å., and G. Nilsson (2005), Drilling of borehole KFM01B at drilling site DS1. *SKB P-report P-04-302.* Svensk Kärnbränslehantering AB.

Claesson, LÅ., and G. Nilsson (2004), Drilling of the telescopic borehole KFM02A at drilling site DS2. *SKB P-report P-04-52*. Svensk Kärnbränslehantering AB.

Cox, J.W., (1970), The high resolution dipmeter reveals a dip related borehole and formation characteristics, *SPWLA Eleventh Annual Logging Symposium, May 3-6, 1970.*

Deltombe, J.-L, and R. Schepers (2004), New development in real-time processing of full waveform acoustic televiewer data. *J. of Applied Geophys., Vol.55, pg.161-172, doi: 10.1016/j.jappgeo.2003.06.013.*

Engelder, T., and M.L Shar (1984), Near-surface in situ stress: Introduction, *J. of Geophys. Research Vol.89 pg. 9321-9322.*

Gustafsson, C., and P. Nilsson (2003), Geophys., radar and BIPS logging in boreholes HFM04, HFM05, and the percussion drilled part of KFM02A. *SKB P-report P-03-53*. Svensk Kärnbranslehantering AB.

Gustafsson, J., and C. Gustafsson (2004), RAMAC and BIPS logging in borehole KFM02A. *SKB P-report P-04-30.* Svensk Kärnbränslehantering AB.

Haimson, B.C., and C.G. Herrick (1985), In situ stress evaluation from borehole breakouts, experimental studies, in E. Ashworth, ed., Research and engineering applications in rock masses.26th U.S. symposium on rock mechanics, South Dakota School of Mines and Technology, Rapid City, 26-28 June, proceedings], *Vol.2, A.A. Balkema, Boston, pg. 1207-1218.*

Haimson, B.C., C.G. Herrick (1986), Borehole breakouts-a new tool for estimating in-situ stress? In: Stephansson, O., ed., Rock stress and rock stress measurements. *International symposium on rock stress and rock stress measurements* [Stockholm, September 1-3], proceedings: Centek Publishers, Stockholm, *pg. 271-280.*

Hakala, M, J. A. Hudson and R. Christiansson (2003), Quality control of overcoring stress measurement data. *Int. J. Rock Mech. Min. Sci. 40 No. 7-8 ,pg. 1141-1159*

Huber, K., K. Fuchs, J. Palmer, E. Roth, B.N. Khakhaev, L.E. Van-Kin, L.A. Pevzner, S. Hickman, D. Moos, M.D. Zoback and D. Schmitt (1997), Analysis of borehole televiewer measurements in the Vorotilov drillhole, Russia - first results. *Tectonophysics, vol. 275 pg. 261-272*

Johansson, P.-O, K. Werner, E. Bosson, S. Berglund, and J. Juston (2005), Description of climate, surface hydrology, and near surface hydrogeology (Preliminary site description Version 1.2), *SKB R-05-06. Svensk Kärnbränslehantering AB.*

Juhlin, C., and M.B. Stephens (2006), Gently dipping fracture zones in Paleoproterozoic metagranite, Sweden-Evidence from reflection seismic and cored borehole data and implications for the disposal of nuclear waste, *J. of Geophys. Res., Vol. 111, B09303, doi, 1029/2005JB003887.*

Leeman, E. R (1964), The measurement of stress in rock, part 1: *J. of the South African Institute of Mining and Metallurgy, vol. 65, pg. 76–80.*

Lindfors, U., F. Perman, and J. Sjöberg (2005), Evaluation of overcoring results from borehole KFM01B. *SKB P-05-66.* Svensk Kärnbränslehantering AB.

Lofts, J.C., and L.T. Bourke (1999), The recognition of artifacts from acoustic and resistivity borehole imaging devices, Borehole Imaging: Applications and case histories, *Geological Society, London, Special Publications, 159, pg. 59-76.*

Ludvigsson, J.E., S. Jönsson, and T. Svensson (2003), Pumping test and flow logging: Boreholes KFM02A (0-100 m), HFM04 and HFM05. *SKB P-03-34,* Svens*k* Kärnbränslenhantering AB.

Mastin, L. (1988), Effects of borehole deviations on breakout orientations, *J. of Geophys. Res., Vol.93, 9187-9195.*

Mattson, H., H. Thunehed, and M. Keisu (2004), Interpretation of borehole Geophysical measurements in KFM01A, KFM01B, HFM01, HFM02, and HFM03, *SKB P-report P-04-80. Svensk Kärnbränslehantering AB.*

Meyer, J. (2002), Determination and Application of In-situ Stresses in Petroleum Exploration and Production, PhD thesis, *National Centre for Petroleum Geology and Geophysics,* University of Adelaide.

Nielsen, U.T., and J. Ringgard (2004a), Geophysical borehole logging in boreholes KFM01B, HFM14, HFM15, HFM16, HFM17, and HFM18. *SKB P-Report P-04-145.* Svensk Kärnbränslehantering AB.

Nielsen, U.T., and J. Ringgard (2004b), Geophysical borehole logging in borehole KFM02A, KFM03A and borehole KFM03B, SKB P-Report P-04-97, Svensk Kärnbränslehantering AB.

Nordgulen, Ø., and A. Braathen (2005), Structural investigations of deformation zones at Forsmark-a pilot study. SKB P-Report P-05-183. *Svensk Kärnbränslehantering AB.*

Nygörd, P. (1999), Overview of the Swedish Repository Program and of the public process for site selections, International Conference on Geologic Repositories, Denver, Colorado

Petersson, J., A. Wägnerud , and A. Stråhle (2003), Boremap mapping of telescopic drilled borehole KFM02A. SKB report P-report P-03-98. *Svensk Kärnbränslehantering AB.*

Plumb, R.A., and S.H. Hickman (1985), Stress-induced borehole enlargement: a comparison between the four-arm dipmeter and the borehole televiewer in the Auburn geothermal well, *J. of Geophys. Res. vol. 90 pg. 5513-5521.*

Reinecker, J., O. Heidbach, M. Tingay, B. Sperner, and B. Müller (2005), The release 2005 of the World Stress Map (available online at **www.world-stress-map.org**)

Reinecker, J., M. Tingay, and B. Müller (2003), Borehole breakout analysis from four-arm caliper logs, Guidelines for interpreting stress indicators (available online at **http://www.world-stress-map.org**).

Reynolds, S.D. (2001), Characterization and modeling of the regional in-situ stress field of continental Australia, PhD thesis, *National Centre for Petroleum Geology and Geophysics*, Adelaide University, Australia

Sano, O., H. Ito, A. Hirata, and Y. Mizuta (2005), Review of methods of measuring stresses and its variations, *Bulletin of Earthquake Res. Institute, University of Tokyo. Vol. 80 pg. 87-103*

Schunnesson, H. (1999), Drilling monitoring of core holes data analysis from core hole KL0023B at Åspö laboratory. *SKB, TD-report TD-99-10*.

Sjöberg, J. (2004), Overcoring rock stress measurements in borehole KFM01B. *SKB P-report P-04-83. Svensk Kärnbränslehantering AB.*

Sjöberg, J., U. Lindfors, Perman F, and D.Ask (2006), Evaluation of the state of stress at the Forsmark site:-Preliminary Site Investigation Forsmark area-Version 1.2. *Svensk Kärnbränslehantering AB* SKB R- report R-05-35. .

SKB (2000), Geoscientific programme for investigation and evaluation of sites for the deep repository. *SKB TR report TR-00-20. Svensk Kärnbränslehantering AB.*

SKB (2004), Preliminary Site Description: - Forsmark area-version 1.1, *Svensk Kärnbränslehantering AB. SKB R-report R-04-14.*

SKB (2005), Preliminary Site Description:- Forsmark area-Version 1.2.Svensk Kärnbränslehantering AB. SKB R-report R-05-18.

Spresnsky, S. (1992), Borehole breakouts and in-situ stress: a review, *The Log Analysts, Vol. 33, pg. 304-312.*

Stacey, T R., and Wasseloo (2002), Application of indirect stress measurement techniques (non strain gauge based technology) to quantify stress environments in mines.

Stephansson, O., C. Ljunngren, and L. Jing (1991), Stress Measurements and tectonic implications for Fennoscandia, *Tectnophysics, vol. 189 pg. 313-322*. Elsevier Science Publishers. B.V., Amsterdam.

Wiprut, D., and M.D. Zoback (2000), Constraining the full stress tensor in the Visund field, Norwegian North Sea: Application of wellbore stability and sand production, *International J. of Rock Mechanic and Mining Sciences, Vol. 37 pg, 317-336k*

Zajac, B.J., and J.M Stock (1997), Using borehole breakouts to constrain the complete stress tensor: - Results from the Sijan Deep Drilling Project and Offshore Santa Maria Basin, California. *J. of Geophys. Res., vol.102, pg 10083 – 10100*.

.

Zemanek, J., and R.L. Cadwell (1967), The Borehole Televiewer- a new logging concept for fracture location and other types of borehole inspection, *J. of Petroleum Technology, Vol. 25 pg. 762-774.*

Zoback, M.D., and M.L. Zoback (1980), State of stress in conterminous United States*, J. of Geophys. Res., Vol. 85 pg. 6113-6156.*

Zoback, M.D., D. Moos, L. Mastin, and R.-N. Anderson (1985), Wellbore breakouts and in situ stress. *J. of Geophys. Res. Vol., 90 pg. 5523–30.*

Zoback, M.D., C.A. Barton, M. Brudy, D.A. Castillo, T. Finkbeiner, B.R. Grollimund, P. Moos, D.B. Peska, C.D. Ward, and D.J. Wiprut (2003), Determination of stress orientation and magnitude in deep wells, *Int J Rock Mech Min Sci vol. 40 pg. 1049-1076,* doi: 10.1016/j.ijrmms.2003.07.001.

Zoback, M. L. (1992), First-and Second-Order Patterns of Stress in the Lithosphere: The *World Stress Map Project, J. Geophys. Res. Vol. 97, No. B8, pp. 11,703-11,728*.

APPENDIX 1

Subdivision of rock unit in borehole KFM01B as was described by *Carlsten et al*., [2004], the author suggested that borehole KFM01B is mainly arock unit but on the basis of degree of fracture frequency, could be sub-divided into two sections as described below:

16-141 m RU1: Medium grained metagranite-granodiorite with subordinate occurrences of fine-to-medium-grained metagranitoids (i.e., granite to granodioritic composition), pegmatic granite and few amphibolites (i.e., amphibolites as a minor rock unit). The interval 92 – 112 m is primarily of fine-to-medium grained metagranitoid.

141-502 m RU1: Medium grained metagranite-granodiorite with subordinate pegmatitic granite, amphibolites and fine-to medium-grained metagranitoid. 202-206 and 222-225 m essentially of fine-to-medium grained granitoid. (See also table 3 and 4 in section 5.3.1 and 5.3.2 for the individual rock units for the section of borehole with breakouts).

In the same vein, *Carlsten et al. [2004]* suggested that borehole KFM01B is associated with three possibly deformation zones as illustrated below:

16-53 m DZ1: Several crush zones and strongly increased frequency of open fractures with most common fracture filling minerals as calcite, chlorite and asphalt. This zone was also described to be associated with a variable degree of oxidation ranging from faint to medium.

107-135 m DZ2: Increased frequency of sealed fractures with epidote and laumontite as dominant fracture filling minerals. Variable degree of oxidation was also reported on this section (ranges from faint to weak).

415-454 m DZ3: presence of two crushed zones and increased frequency of sealed fractures with calcite, laumontite, chlorite and prehenite as dominant filling minerals. Variable degree of oxidation ranging from faint to strong was also reported on this section.

Appendix 2

Subdivision of rock unit in borehole KFM02A as was described by *Carlsten et. al. [2004]*. The author suggested that borehole KFM02A comprises of fourrock unit but on the basis of occurrence of subordinate rock type can be subdivided into 16 rock units as described below:

100-155 m RU1a: Medium-grained metagranite to granodiorite with subordinate occurrences of amphibolite and pegmatitic granite.

155-205 m RU2a: Heterogeneous interval, predominantly with a fine-grained metagranitoid. The second most abundant bedrock component is the medium-grained Metagranite -granodiorite, and then the amphibolite. The central part of the interval is strongly oxidised with three minor intervals of vuggy metagranitoid.

205-240 m RU1b: Occurred as the same dominant rock unit as between 100-155 m depth, with one about 5m wide occurrence of fine-grained metagranitoid and several minor occurrences of pegmatitic granite.

240-310 m RU3: Vuggy metagranite subjected to a strong albite-hematite-chlorite alteration with some minor occurrences of fine-grained metagranitoid, amphibolite and pegmatitic granite.

310-485 m RU1c: Same dominant rock as between 100-155 m depth, with one about 8 m wide occurrence of fine-grained metagranitoid, one about 3 m wide amphibolite and some minor occurrences of pegmatitic granite, fine-grained metagranite and amphibolites.

485-520 m RU2b: Heterogeneous interval, predominantly with the fine-grained metagranitoid. The second most abundant rock unit is the metagranite-granodiorite, and then pegmatitic granite. Also some subordinate amphibolites. Most of the interval has been subjected to a variable degree of oxidation.

520-540 m RU1d: Same dominant rock as between 100-155 m depth, with several minor occurrences of pegmatitic granite and amphibolite. To a variable extent oxidised.

540-575 m RU2c: The upper two thirds of the interval consist of fine-grained metagranite, whereas the lower third is more heterogeneous and composed of amphibolite, pegmatitic granite and the medium-grained metagranite-granodiorite.

575-600 m RU1e: Same dominant rock as between 100-155 m depth.

600-635 m RU2d: Fine-grained metagranite and the medium-gained metagranite-granodiorite in approximately equal proportions with some minor occurrence of pegmatitic-granite.

635-835 m RU1f: Same dominant rock as between 100-155 m depth, with some up to 8m wide occurrences of fine-grained metagranitoid, amphibolite and pegmatitic granite. The uppermost part of the interval has been subjected to a variable extent of oxidation.

835-86 7m RU2e: Heterogeneous interval, predominantly with the fine-grained metagranitoid, and then the medium-grained metagranite-granodiorite and amphibolite. Also some subordinate occurrences of pegmatitic granite.

867-903 m RU1g: Same dominant rock as between 100-155 m depth, with several minor occurrences of pegmatitic granite, up to about 1.5 m in width.

903-938 m RU4: A homogeneous interval of a tonalitic variety of the fine-grained metagranitoid. Also occur along with some minor amphibolite and pegmatitic granite.

938-1001 m RU1h: Same dominant rock as between 100-155 m depth, with several minor occurrences of pegmatitic granite and amphibolite.

Below are the suggested ten possibly deformation zones in borehole KFM02A as described by *Carlsten et al. [2004]*:

79-91 m DZ1: Possible zone which actually consists of three more well-defined sites with increased fracture aperture. Slightly higher fracture frequency close to the lowest site.

110-122 m DZ2: Increased frequency of open fractures, often measurable apertures and calcite coating. Includes several crush zones.

160-184 m DZ3: Increased frequency of both sealed and open fractures, some with measurable apertures. Typically chlorite and/or calcite coated fractures. Most of the interval is more or less strongly oxidised with three minor occurrences of vuggy metagranite.

266-267m DZ4: Crush zone.

303-310 m DZ5: Increased frequency of sealed, but to some extent also open fractures. Typically chlorite and/or calcite coated fractures. Most of the interval is more or less strongly oxidised.

415-520 m DZ6: A With a wide zone consisting of increased frequency of both open and sealed fractures. Typically chlorite and/or calcite coated fractures.

520-600m DZ7: A zone characterised by an increased frequency of sealed fractures, but relatively few open fractures. Consist of mainly epidote sealing and oxidised wall rock.

893-905m DZ8: Increased frequency of open fractures, often with measurable apertures and calcite and/or chlorite coating.

922-925m DZ9: Similar to the 893-905 m interval, but also with an increased frequency of sealed fractures. This interval is assumed to be a contact point within various minor rock occurrences of pegmatite granite and amphibolites.

976-982m DZ10: Slightly increased frequency of both open and sealed fractures consisting of mainly calcite and chlorite coatings.